




ORIGINAL RESEARCH

# Neuraminidases 1 and 3 Trigger Atherosclerosis by Desialylating Low-Density Lipoproteins and Increasing Their Uptake by Macrophages

Ekaterina P. Demina, PhD\*; Victoria Smutova, PhD\*; Xuefang Pan, PhD; Anne Fougerat, PhD; Tianlin Guo, PhD; Chunxia Zou, MSc; Radhika Chakraborty, MSc; Brendan D. Snarr, PhD; Tze C. Shiao, MSc; Rene Roy, PhD; Alexander N. Orekhov, PhD; Taeko Miyagi, PhD; Muriel Laffargue, PhD; Donald C. Sheppard , MD; Christopher W. Cairo, PhD ; Alexey V. Pshezhetsky , PhD

**BACKGROUND:** Chronic vascular disease atherosclerosis starts with an uptake of atherogenic modified low-density lipoproteins (LDLs) by resident macrophages, resulting in formation of arterial fatty streaks and eventually atheromatous plaques. Increased plasma sialic acid levels, increased neuraminidase activity, and reduced sialic acid LDL content have been previously associated with atherosclerosis and coronary artery disease in human patients, but the mechanism underlying this association has not been explored.

**METHODS AND RESULTS:** We tested the hypothesis that neuraminidases contribute to development of atherosclerosis by removing sialic acid residues from glycan chains of the LDL glycoprotein and glycolipids. Atherosclerosis progression was investigated in apolipoprotein E and LDL receptor knockout mice with genetic deficiency of neuraminidases 1, 3, and 4 or those treated with specific neuraminidase inhibitors. We show that desialylation of the LDL glycoprotein, apolipoprotein B 100, by human neuraminidases 1 and 3 increases the uptake of human LDL by human cultured macrophages and by macrophages in aortic root lesions in *ApoE*<sup>-/-</sup> mice via asialoglycoprotein receptor 1. Genetic inactivation or pharmacological inhibition of neuraminidases 1 and 3 significantly delays formation of fatty streaks in the aortic root without affecting the plasma cholesterol and LDL levels in *ApoE*<sup>-/-</sup> and *Ldlr*<sup>-/-</sup> mouse models of atherosclerosis.

**CONCLUSIONS:** Together, our results suggest that neuraminidases 1 and 3 trigger the initial phase of atherosclerosis and formation of aortic fatty streaks by desialylating LDL and increasing their uptake by resident macrophages.

**Key Words:** Ashwell-Morell receptor ■ low-density lipoprotein ■ macrophage ■ neuraminidase ■ sialic acid

**A**therosclerosis, a chronic inflammatory disorder of the medium and large arteries, is currently the most common cause of heart attacks, strokes, and vascular disease. Atherosclerosis manifests with endothelial disruption, inflammatory cascade,

migration of monocytes into the tunica media, proliferation of smooth muscle cells, and formation of atheromatous plaques, occurring initially at the sites of reduced blood flow. Previous studies have identified a vast number of risk factors contributing to

Correspondence to: Alexey V. Pshezhetsky, PhD, Sainte-Justine University Hospital Research Center, 3175 Cote Ste-Catherine, Montreal, QC H3T 1C5, Canada. E-mail: alexei.pchejetski@umontreal.ca and Christopher W. Cairo, PhD, Department of Chemistry, 4-082 Centennial Centre for Interdisciplinary Science, University of Alberta, Edmonton, AB T6G 2G2, Canada. E-mail: ccairo@ualberta.ca

\*Dr Demina and Dr Smutova contributed equally to this work as co-first authors.

Anne Fougerat is currently located at the Institut National de la Recherche Agronomique, ToxAlim, UMR1331 Toulouse, France.

Supplementary Material for this article is available at <https://www.ahajournals.org/doi/suppl/10.1161/JAHA.120.018756>

For Sources of Funding and Disclosures, see page 21.

© 2021 The Authors. Published on behalf of the American Heart Association, Inc., by Wiley. This is an open access article under the terms of the Creative Commons Attribution-NonCommercial License, which permits use, distribution and reproduction in any medium, provided the original work is properly cited and is not used for commercial purposes.

JAHA is available at: [www.ahajournals.org/journal/jaha](http://www.ahajournals.org/journal/jaha)

## CLINICAL PERSPECTIVE

### What Is New?

- In this article, we explore the role of neuraminidase enzymes in the development of atherosclerosis.
- We demonstrated that neuraminidases 1 and 3 remove sialic acids from circulating low-density lipoprotein, leading to increased uptake by macrophages in the arterial intima via the asialoglycoprotein receptor 1.
- We further showed that genetic inactivation or pharmacological inhibition of neuraminidases 1 and 3 in apolipoprotein E or low-density lipoprotein receptor knockout mice significantly delays formation of aortic root fatty streaks without affecting plasma cholesterol and low-density lipoprotein levels.

### What Are the Clinical Implications?

- The clinical implications of this study include the discovery of a novel pathway involved in the development of atherosclerosis, one of the most important causes of cardiovascular mortality, and the identification of novel, potentially drug-gable targets that can prevent atherosclerosis independent of cholesterol levels.

## Nonstandard Abbreviations and Acronyms

<b>ASGR</b>	asialoglycoprotein receptor
<b>BMDM</b>	bone marrow–derived macrophage
<b>BW</b>	body weight
<b>DANA</b>	2,3-didehydro-2-deoxy-N-acetylneuraminic acid
<b>desLDL</b>	desialylated low-density lipoprotein
<b>DMSO</b>	dimethyl sulfoxide
<b>LC</b>	liquid chromatography
<b>LDLR</b>	low-density lipoprotein receptor
<b>MS</b>	mass spectrometry
<b>NEU1</b>	neuraminidase 1
<b>NEU3</b>	neuraminidase 3
<b>NEU4</b>	neuraminidase 4
<b>oxLDL</b>	oxidized low-density lipoprotein
<b>Sia</b>	sialic acid
<b>WT</b>	wild type

atherosclerosis in the human population, including hyperlipidemia, smoking, hypertension, genetic predisposition, age, sex, and obesity.<sup>1</sup> However, the cellular, biochemical, and molecular mechanisms underlying plaque development are still not fully understood. Activation of endothelial cells plays a critical role in the initiation and progression of atherosclerosis,

leading to secretion of proinflammatory cytokines and chemokines, and increased expression of the adhesion surface molecules. These factors result in leukocyte adhesion and migration into the subendothelial space, where they differentiate into residential macrophages.<sup>2</sup> Subsequently, these macrophages recognize and take up low-density lipoproteins (LDLs) that infiltrate from the circulation into the subendothelial space of the arterial wall. Uptake of LDLs by macrophages leads to an uncontrolled accumulation of cholesterol, and their conversion to foam cells, which triggers a cascade of immune responses that collectively lead to atheroma formation.<sup>3</sup>

High levels of circulating cholesterol associated with LDL particles are a well-known risk factor for development and progression of atherosclerosis. However, as many as 46% of initial cardiovascular events occur in people with LDL levels within the normal range,<sup>4</sup> suggesting that other factors are also important for triggering atherosclerosis. One possible mechanism underlying the development of atherosclerosis in this population is the alteration of LDL particle composition, through chemical or enzymatic modification. Oxidation or acetylation of LDL lipids *in vitro* allows these particles to become ligands of scavenger receptors on the surface of macrophages and increases their uptake. However, it remains unclear whether oxidation and acetylation are the primary atherogenic LDL modifications *in vivo* or if other types of modifications play equal or more important roles. One such candidate modification is desialylation: the removal of terminal sialic acids (Sia; also called N-acetylneuraminic acid or Neu5Ac) from the glycan chains associated with LDL glycoproteins and glycolipids. Sialylation plays an important role in the biological features of LDLs; all LDL particles contain sialylated glycoproteins and G<sub>M2</sub> ganglioside molecules.<sup>5,6</sup> In particular, the core protein of human plasma LDL, apolipoprotein B 100 (ApoB), contains from 12 to 14 sialic acid residues as a part of its N-linked glycans.<sup>5</sup> In contrast to oxidation, desialylation of LDL occurs naturally through the action of neuraminidase enzymes. It has been shown that Sia content of LDLs in patients with coronary artery disease and atherosclerosis is lower than that in healthy subjects,<sup>7,8</sup> whereas the blood levels of free Sia are increased.<sup>9</sup> Desialylated LDLs are rapidly taken up by and accumulate within peripheral blood macrophages and smooth muscle cells isolated from the human arterial intima.<sup>10</sup> Desialylation of LDL causes changes in the structure of ApoB and results in accumulation of neutral lipids and cholesteryl esters in human aortic intimal cells.<sup>11</sup>

In the present work, we describe a novel pathological pathway active during the early stages of atherosclerosis, in which neuraminidases desialylate circulating LDLs, leading to increased uptake of these particles by macrophages. Enzymes of neuraminidase (also called

sialidase) family are encoded in mammals by the *Neu1-Neu4* genes. Neuraminidase 1 (NEU1) to neuraminidase 4 (NEU4) catalyze the removal of terminal sialic acids from glycoproteins, oligosaccharides, and glycolipids, and have distinct, yet overlapping, tissue expression, intracellular localization, and substrate specificity. They play important physiological roles, regulating immune response, cell proliferation, metabolism, normal development, and carcinogenesis by desialylation of a wide spectrum of physiological substrates. Our current results demonstrate that genetic inactivation or pharmacological inhibition of NEU1 and neuraminidase 3 (NEU3) significantly delays formation of fatty streaks in the aortic root without affecting the plasma cholesterol and LDL levels in *ApoE*<sup>-/-</sup> or *Ldlr*<sup>-/-</sup> mice, suggesting that these enzymes trigger the initial phase of atherosclerosis.

## METHODS

All data and analytical methods are included in the article and its online supplementary files (Data S1). The study materials will be made available to other researchers for purposes of reproducing the results or replicating the procedure on request to the corresponding authors.

### Production and Purification of Human NEU1 to NEU4

Human recombinant neuraminidase 2, NEU3, and NEU4 were expressed as N-terminal maltose binding protein fusion proteins in *Escherichia coli* and purified as previously reported.<sup>12</sup> Because production of active recombinant NEU1 requires mammalian cells, the human enzyme was expressed as a His-tagged protein in HEK293 cells, transduced with a CathA-IRES-NEU1 lentivirus,<sup>13</sup> and partially purified by affinity chromatography using HisPur Ni-NTA (Thermo Fisher Scientific; 88222). For lectin blotting experiments, commercially available purified recombinant human NEU1 (NEU1-156H; Creative Biomart) was used. Neuraminidase activity and inhibition assays were performed using 2'-(4-methylumbelliferyl)- $\alpha$ -D-N-acetylneuraminic acid and GM3 ganglioside as substrates, as described.<sup>14</sup>

### Isolation of LDL and Lipoprotein-Deficient Serum

Approval for collection and use of human blood samples was granted by the Research Ethics Board of Ste-Justine University Hospital Centre (CHU Ste-Justine). LDL fraction (density between 1.020 and 1.063 g/mL) was isolated from EDTA-anticoagulated blood plasma, obtained from healthy normolipidemic human donors by density gradient ultracentrifugation, as described.<sup>15</sup> Purity of the isolated LDL fraction was confirmed by

PAGE analysis, which detected a single 500-kDa ApoB protein band. The isolated LDL fraction was dialyzed against PBS containing 1 mmol/L EDTA at 4°C. Human lipoprotein-deficient serum was prepared by ultracentrifugation of a serum at a density of 1.25 g/mL<sup>15</sup> followed by dialysis against PBS at 4°C. Protein concentration was measured using Quick Start Bradford Protein Assay (Bio-Rad; 5000201). Mouse LDL fraction was isolated, as described above, from pooled blood collected by cardiac puncture from ten 16-week-old mice.

### LDL Modification and Labeling

Isolated LDL (300  $\mu$ L; 2.3 mg/mL in PBS) was supplemented with 60  $\mu$ L of the reaction buffer (0.1 mol/L NaOAc and 10 mmol/L CaCl<sub>2</sub>) with optimal pH for each enzyme<sup>14</sup> and desialylated with human recombinant neuraminidases<sup>16</sup> (1–2 mU of enzyme/10  $\mu$ g of LDL). The reaction mixture was supplemented with protease inhibitor cocktail (cComplete ULTRA Tablets; Roche). The reaction was continued at 37°C for 3 hours with a constant shaking and stopped by adding 0.1 mol/L Na<sub>2</sub>CO<sub>3</sub> buffer, pH 7.4. Desialylation of LDL was confirmed by lectin blot or liquid chromatography (LC) with tandem mass spectrometry (MS/MS), as described below. To prepare oxidized LDL, the sample was dialyzed against PBS supplemented with CuSO<sub>4</sub> (5  $\mu$ mol/L, final concentration) and incubated at 37°C for 24 hours.

Native or modified LDL was labeled with a fluorescent 3,3'-dioctadecylindocarbocyanine dye (Molecular Probes), as described,<sup>17</sup> with minor modifications. Briefly, 100  $\mu$ L of dye, dissolved in dimethyl sulfoxide (DMSO) at a concentration of 3 mg/mL, was added to 2 mL of lipoprotein-deficient serum containing 1 mg of LDL. After incubation at 37°C for 24 hours in the dark, KBr powder was added to adjust the density of the mixture to 1.063 g/mL, and LDL was reisolated by ultracentrifugation. Labeling of native or modified LDL with Alexa Fluor 488 or 594 (Invitrogen) was performed following the manufacturer's protocol. After labeling, LDL samples were dialyzed against PBS, filtered (0.22- $\mu$ m pore size) before each experiment, and used within 2 weeks after isolation.

### Lectin Blotting

LDL samples were subjected to NuPAGE using 3% to 8% Novex Bis-Tris gels (Invitrogen) and transferred to nitrocellulose membrane. Blots were blocked with 50 mmol/L Tris-HCl, pH 7.4, containing 150 mmol/L NaCl, 3% (w/v) BSA, and 0.05% Tween 20 at room temperature for 1 hour, and then incubated overnight with biotinylated *Maackia amurensis* lectin-II, *Sambucus nigra* lectin, or peanut (*Arachis hypogaea*) agglutinin (Vector Laboratories) in the same buffer containing 1%

BSA at 4°C. After washing with Tris-buffered saline–Tween (0.05% v/v), blots were incubated with horseradish peroxidase–conjugated streptavidin for 1 hour at room temperature. Following washing with Tris-buffered saline–Tween, blots were developed using ECL chemiluminescence reagent (Thermo Fisher Scientific) and analyzed using x-ray film. Ponceau S–stained membranes were used as a control for equal protein loading.

### Analysis of LDL Uptake by Cultured Macrophages and HepG2 Cells

Human peripheral blood mononuclear cells were isolated from the blood of immunodeficiency virus type 1/hepatitis B and C seronegative donors by centrifugation over Ficoll–Paque Plus (Amersham Biosciences) gradient. Monocytes were further isolated using EasySep Human Monocyte Isolation Kit (Stemcell). Cells were plated at a density of  $2 \times 10^5$  monocytes per  $\text{cm}^2$  on glass coverslips in 24-well plates and cultured in RPMI 1640 medium containing 10% fetal bovine serum, 1% antibiotic antimycotic, and 20 ng/mL of human recombinant macrophage colony-stimulating factor (eBioscience). After 7 days in culture, differentiated macrophages (larger and more granular than monocytes, as visualized by light microscopy) were confirmed to have characteristic macrophage cell surface phenotypic markers (cluster of differentiation [CD] 14 and CD206) by flow cytometry. Mouse bone marrow–derived macrophages (BMDMs) and peritoneal macrophages from wild-type (WT), *Asgpr1*<sup>−/−</sup>, and *Gal3*<sup>−/−</sup> mice were produced, as previously described.<sup>18,19</sup>

Human monocyte-derived macrophages and mouse BMDMs and peritoneal macrophages grown on glass coverslips were cultured overnight in RPMI 1640 medium, containing 5% (v/v) lipoprotein-deficient serum; then, the medium was supplemented with labeled LDL (30  $\mu\text{g}/\text{mL}$ , final concentration) and the cells were incubated further for 3 hours at 37°C. To study the competition between the uptake of desialylated and oxidized LDL, macrophages were incubated for 3 hours with 30  $\mu\text{g}/\text{mL}$  of 3,3′-dioctadecylindocarbocyanine–labeled oxidized or desialylated LDL in the absence or in the presence of 5-, 10-, or 20-fold excess of nonlabeled oxidized or desialylated LDL. To study the uptake of LDL by HepG2, the cells grown on glass coverslips coated with poly-L-lysine were incubated for 20 minutes in DMEM containing 5% lipoprotein-deficient serum and 30  $\mu\text{g}/\text{mL}$  of native or modified and labeled LDL. After incubation, all cells were washed three times with ice-cold PBS and incubated on ice with 2 mg/mL of heparin (Sigma-Aldrich; H3149) in PBS for 2 hours. Cells were further rinsed with PBS and fixed for 20 minutes with 4% paraformaldehyde/4%

sucrose solution on ice. The coverslips were mounted onto slides with ProLong Gold antifade reagent (ThermoFisher; P36930) and analyzed by confocal fluorescence microscopy using a Leica DM 5500 Q upright microscope ( $\times 40$  dry objective).

### Animals

Approval for animal experimentation was granted by the Animal Care and Use Committee of the Ste-Justine Hospital Research Center. Mice were housed in an enriched environment with continuous access to food and water, under constant temperature and humidity, on a 12-hour light/dark cycle. Mice were kept on a normal chow diet (5% fat, 57% carbohydrate) unless indicated otherwise. *Neu4*<sup>−/−</sup>, *Neu3*<sup>−/−</sup>, and NEU1-deficient (*CathA*<sup>S190A-Neo</sup>) mice have been described before.<sup>20–22</sup> *Asgr1*<sup>−/−</sup> (B6.129S4-Asgr1tm1Sau/SaubJxmJ; The Jackson Laboratory [JAX] stock No. 009105), *ApoE*<sup>−/−</sup> (B6.129P2-ApoE<sup>tm1Unc</sup>/J; JAX stock No. 002052), *Gal3*<sup>−/−</sup> (B6.Cg-Lgals3tm1Poi/J; JAX stock No. 006338), and *Ldlr*<sup>−/−</sup> (B6.129S7-Ldlr<sup>tm1Her</sup>/J; JAX stock No. 002207) were obtained from JAX (Bar Harbor, ME).

### Analysis of LDL Incorporation in the Mouse Aortic Wall and Liver

Tissue incorporation of LDL in vivo was studied essentially as described by Chang et al.<sup>23</sup> Sixteen-week-old C57Bl6 mice were injected through the tail vein with 200  $\mu\text{g}$  of native or desialylated Alexa 488- or 3,3′-dioctadecylindocarbocyanine–labeled LDL in 100  $\mu\text{L}$  of saline (3–4 males, 3–4 females for each group). Six hours after injection, mice were euthanized and perfused with 4% paraformaldehyde solution. Accumulation of Alexa or 3,3′-dioctadecylindocarbocyanine was quantified on cross-sections of the liver and the aorta starting at the level of the aortic root. For that, isolated organs were embedded with optimum cutting temperature compound (Tissue-Tek). Forty sections with 10- $\mu\text{m}$  thickness were prepared from the top of the left ventricle, where the aortic valves were first visible, up to the position in the aorta where the valve cusps were just disappearing from the field. Tissue autofluorescence was reduced by treatment with TrueBlack reagent (Biotium; 23012-T) using the protocol of the manufacturer, and the Alexa fluorescence was analyzed using a Leica DM 5500 Q upright confocal microscope ( $\times 40$  or  $\times 63$  dry objective). The captured images were quantified using ImageJ software. To access colocalization of Alexa labels with asialoglycoprotein receptor (ASGR) 1, NEU1, and CD68, tissues were postfixed with 4% paraformaldehyde, sectioned, and stained with the corresponding antibodies (anti-ASGR1 antibody, rabbit polyclonal, Proteintech, 11739-1-AP, dilution 1:200; anti-NEU1 antibody, rabbit polyclonal, Abcam,

ab233119, dilution 1:200; and anti-CD68 antibody, rabbit polyclonal, Abcam, ab125212, dilution 1:200), essentially as described.<sup>24</sup>

### Analysis of Atherosclerotic Lesions in *Apoe*<sup>-/-</sup> Mice Deficient in NEU1, NEU3, or NEU4

To generate *Apoe*<sup>-/-</sup> mice with deficiencies of NEU1, NEU3, and NEU4, *Apoe*<sup>-/-</sup> (B6.129P2-*Apoe*<sup>tm1Unc/J</sup>; JAX) mice were crossed with previously described *Neu3*<sup>-/-</sup>, *Neu4*<sup>-/-</sup>, or *CathA*<sup>S190A-Neo</sup> mice. All mice had the same C57Bl/6J genetic background. Between 8 and 20 female mice were analyzed for each genotype.

At the age of 16 weeks, mice were euthanized and areas of atherosclerotic lesions in aortic root were analyzed, as described previously.<sup>25</sup> Briefly, isolated hearts were washed and incubated overnight in PBS at 4°C. The upper cardiac portion (aortic root) was embedded in optimum cutting temperature compound and cut into sequential 10- $\mu$ m-thick cross-sections by a Leica CM1950 Cryostat (Leica Microsystems, Wetzlar, Germany). Five of the frozen sequential cross-sections covering a distance of 500  $\mu$ m were collected on a glass slide. The neutral lipids in the plaques of the aortic root were stained red by Oil Red O and further quantified. Slides were counterstained with hematoxylin (MHS16; Sigma-Aldrich), dried, and mounted with VectaMount medium (H-5501; Vector Laboratories). The intima lesion size was expressed as  $\mu$ m<sup>2</sup>. Surface lesion area at the aortic root was measured by computer-assisted image quantification after staining with Oil Red O by an operator blinded for the mouse genotype or treatment.

To analyze inflammatory cell infiltration within atherosclerotic lesions, frozen sections from the aortic root were air dried, fixed in acetone/methanol (1:1) mix, and incubated with 3% hydrogen peroxide in methanol for 10 minutes to eliminate endogenous peroxidase. The sections were then blocked in 3% BSA for 30 minutes and in 2% normal rabbit serum (Vector Laboratories) for 3 minutes. The sections were further stained with either rat monoclonal anti-mouse macrophage antibody (clone anti-macrophage antibody; Serotec; 1:50 dilution) or goat polyclonal anti-mouse CD3 antibody (clone M-20; Santa Cruz Biotechnology; 1:200 dilution), both in 2% mouse serum. Then, sections were incubated with corresponding secondary biotinylated antibodies (Vector Laboratories) in 3% BSA and visualized with a streptavidin horseradish peroxidase complex (Sigma) and 3, 3'-diaminobenzidine peroxidase substrate (Sigma). Counterstaining was performed using the Mayer hematoxylin method.

LDL, cholesterol, triglyceride, and high-density lipoprotein (HDL) levels in the mouse plasma were measured in the CHU Ste-Justine central biochemistry

laboratory or by Charles River Inc using the enzymatic methods, as described by Allain<sup>26</sup> and Roeschlau,<sup>27</sup> respectively.

### Pharmacological Inhibition of NEU1 and NEU3 in *Apoe*<sup>-/-</sup> Mice

Specific inhibitors of human neuraminidase enzymes were synthesized and characterized, as previously described, and their specificity was confirmed with mouse NEU orthologs.<sup>12</sup> Twelve week-old *Apoe*<sup>-/-</sup> female mice, fed normal diet, received intraperitoneal injections of sterile solutions of C9-butyl-N-amide-DANA (C9-BA-DANA) (30 mg/kg body weight [BW]; n=6), CG22601 (10 mg/kg BW; n=6), and CG14601 (10 mg/kg BW; n=5) in saline or CG17701 (1 mg/kg BW; n=6) in saline containing 2% (v/v) DMSO every 48 hours for 2 weeks. All inhibitors were used as the C1-methyl esters. The frequency of injections was then increased to every 24 hours for another 2 weeks. Saline-treated (n=15) and 2% DMSO-treated mice (n=5) were used as controls. At the age of 16 weeks, mice were euthanized and areas of fatty streaks in aortic root within atherosclerotic lesions were analyzed, as described above.

### Pharmacological Inhibition of NEU1 and NEU3 in *Ldlr*<sup>-/-</sup> Mice

Starting from the age of 8 weeks, female *Ldlr*<sup>-/-</sup> mice (B6.129S7-*Ldlr*<sup>tm1Her/J</sup> mouse strain; JAX stock No. 002207) were fed a proatherogenic diet containing 15% fat, 1.25% cholesterol, and 0% cholate (TD.96335 modified; Envigo). From 10 weeks, mice were receiving intraperitoneal injections of sterile solutions of CG22601 (10 mg/kg BW; n=9) and CG14601 (10 mg/kg BW; n=8) in saline every 48 hours for 2 weeks. The frequency of the injections was then increased to every 24 hours for another 2 weeks. Saline-treated mice were used as controls (n=7). After 4 weeks of treatment, mice were euthanized and areas of fatty streaks in aortic root were analyzed, as described above for *Apoe*<sup>-/-</sup> mice.

### Histochemical Assay of Neuraminidase Activity in Mouse Kidney Tissues

Sections that were 10  $\mu$ m thick were cut from optimum cutting temperature-embedded frozen mouse kidney using a CM3050 S Microtome (Leica). The slices were incubated with 0.2 mmol/L 1,5-bromo-4-chloroindol-3-yl-5-acetamido-3,5-dideoxy- $\alpha$ -D-glycero-D-galacto-2-nonulopyranosidonic acid (X-Neu5Ac; Sigma) and Fast Red Violet LB Salt (Sigma), at pH 4.7 for 1 hour. Sections were then rinsed in PBS, mounted onto glass slides using Vectashield mounting medium, and scanned using Axioscan slide scanner (Zeiss).

## Glycopeptide Analysis

LDL samples (50  $\mu$ L) were mixed with a solution of 4:3:1 methanol/water/chloroform (400  $\mu$ L) and centrifuged (10 000g, 2 minutes). The upper phase was carefully removed and replaced with 200  $\mu$ L of methanol. The sample was vortexed for 10 seconds and then centrifuged at 10 000g for 2 minutes. The supernatant was removed, and the pellet was washed again with methanol, dried under vacuum, dissolved in ammonium bicarbonate buffer, pH 8.0, and digested with Proteinase K, at 37°C, overnight. Samples were then dried, and the digested glycopeptides were enriched using a ProteoExtract Glycopeptide Enrichment Kit (Novagen), following the manufacturer's protocol. Samples were analyzed on Waters QTOF Premier mass spectrometer equipped with a Waters nanoAcquity ultraperformance LC system with peptide trap column (180  $\mu$ m $\times$ 20 mm; Symmetry C18 nanoAcquity; Waters, Milford, MA) and an analytical column (75  $\mu$ m $\times$ 150 mm; Atlantis dC18 nanoAcquity; Waters). The data file was processed with ProteinScope 3.1 (Waters) and Findpep tool on the EXPASY website.

## N-Glycan Profiling of LDL Samples by LC-MS

Profiles of released N-glycans were generated using a GlycoWorks RapiFluor-MS N-Glycan kit (Waters), following the manufacturer's protocol. LC with fluorescence detection (265 nm excitation/465 nm emission) and MS (high-performance LC [HPLC]–fluorescence detector–MS) were performed using an Agilent 1200 SL HPLC System and a Glycan PAC AXH-1 analytical column, 2.1 $\times$ 150 mm, 1.9- $\mu$ m particle size (Thermo Scientific), with a precolumn, at 40°C. Mass spectra were acquired in positive mode of ionization using

an Agilent 6220 Accurate-Mass TOF [Time-of-Flight] HPLC/MS system (Agilent, Santa Clara, CA), equipped with a dual sprayer electrospray ionization source with the second sprayer providing a reference mass solution. Data analysis was performed using the Agilent MassHunter Qualitative Analysis software package version B.07.01.

## Analysis of Gangliosides From Mouse Plasma

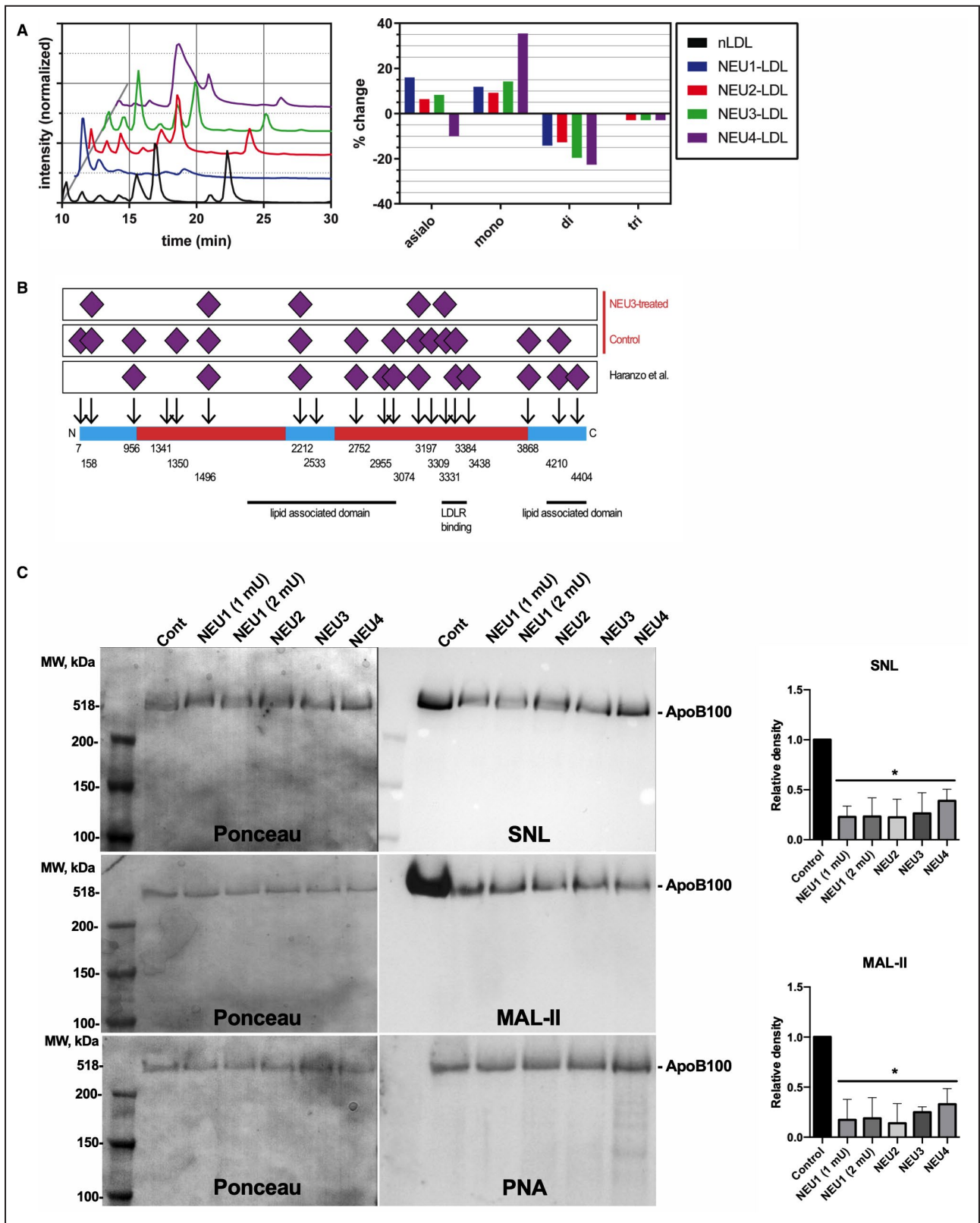
Recombinant EGCCase was produced and purified, as described by Albrecht et al.<sup>28</sup> Gangliosides were extracted and purified, as described,<sup>29</sup> and analyzed, as described by Neville et al.<sup>30</sup> Briefly, gangliosides were incubated for 18 hours at 30°C with 0.086 U of EGCCase and released glycans were labeled with 2-anthranilic acid. Labeled glycans were analyzed by LC-MS using an Agilent 1200 SL HPLC system and a normal-phase column (Accucore-150-Amide-HILIC; 2.6  $\mu$ m; 2.1 $\times$ 150 mm; Thermo Fisher) at 40°C. Relative glycan concentrations were quantified using fluorescence detection (excitation at 320 nm/emission at 420 nm), and peak areas were normalized to the internal standard, maltose. Mass spectra were acquired in negative mode using an Agilent 6220 Accurate-Mass TOF HPLC/MS system with a dual-spray electrospray ionization source along with a secondary reference sprayer. Data analysis was performed using the Agilent MassHunter Qualitative Analysis software package version B.07.01.

## Statistical Analysis

Statistical analyses were performed using Prism GraphPad 9.0.0. software (GraphPad Software, San Diego, CA). The normality for all data was checked using the D'Agostino and Pearson omnibus normality

### Figure 1. Human neuraminidases remove sialic acids from the glycan chains of apolipoprotein B 100 (ApoB) in human low-density lipoprotein (LDL).

**A**, Liquid chromatography–mass spectrometry (LC-MS) profiles of ApoB N-glycans from neuraminidase-treated and untreated human LDL. Chromatograms of fluorescently labeled N-glycans cleaved from ApoB of human LDL from a healthy donor (black) and of LDL treated with recombinant human neuraminidase 1 (NEU1), neuraminidase 2 (NEU2), neuraminidase 3 (NEU3), and neuraminidase 4 (NEU4) enzymes (blue, red, green, and purple, respectively). Samples were resolved on an anion exchange column, where glycans with higher sialic acid content are eluted at later retention times. For all samples, the intensities were normalized to those of the corresponding peaks of asialo glycans (10–11 minutes retention time). Figure shows representative profiles of duplicate experiments. Quantitation of peak areas and glycan assignment is shown in Tables S3 and S4. Bar graph shows relative changes in the asialo-side, monosialo-side (mono), disialo-side (di), and trisialo-side (tri) N-glycan profiles for the neuraminidase-treated compared with untreated LDL on the basis of the analysis of the corresponding MS/MS fragmentation patterns. **B**, Neu5Ac-containing glycopeptides identified on ApoB. Purified LDL was treated with recombinant NEU3 enzyme or a buffer control, and the ApoB glycoprotein was resolved by SDS-PAGE, digested with proteinase K, and analyzed by LC-MS/MS to identify glycopeptides. A map of the primary protein sequence is shown (bottom) with the  $\alpha$  (blue) and  $\beta$  (red) domains highlighted. Arrows indicate predicted sites of N-linked glycosylation, with the numbers of the glycosylated asparagine residues shown below the protein map. Diamonds indicate detected glycopeptides containing at least one sialic acid. Data from Harazono et al<sup>76</sup> are shown for comparison. Identified glycopeptides are shown in Tables S3 and S4. **C**, ApoB in neuraminidase-treated LDL shows reduced staining with *Sambucus nigra* lectin (SNL) and *Maackia amurensis* lectin (MAL)-II lectins and is recognized by peanut (*Arachis hypogaea*) agglutinin (PNA) lectin, consistent with its desialylation. Purified human LDLs (10  $\mu$ g) were incubated with human recombinant NEU1 (1 and 2 mU), NEU2 (1 mU), NEU3 (1 mU), or NEU4 (1 mU), and glycosylation of ApoB was analyzed by blotting with SNL, MAL-II, or PNA lectin. Ponceau S–stained membranes were used as controls for protein loading. Cont indicates control; LDLR, LDL receptor; MW, molecular weight; and nLDL, native LDL. \* $P$ <0.05 compared with control in ANOVA test (n=3).



test. Significance of the difference was determined using *t*-test (normal distribution) or Mann-Whitney test, when comparing 2 groups. One-way ANOVA test,

followed by the Tukey multiple comparison test (normal distribution), or Kruskal-Wallis test, followed by the Dunn multiple comparison test, was used when

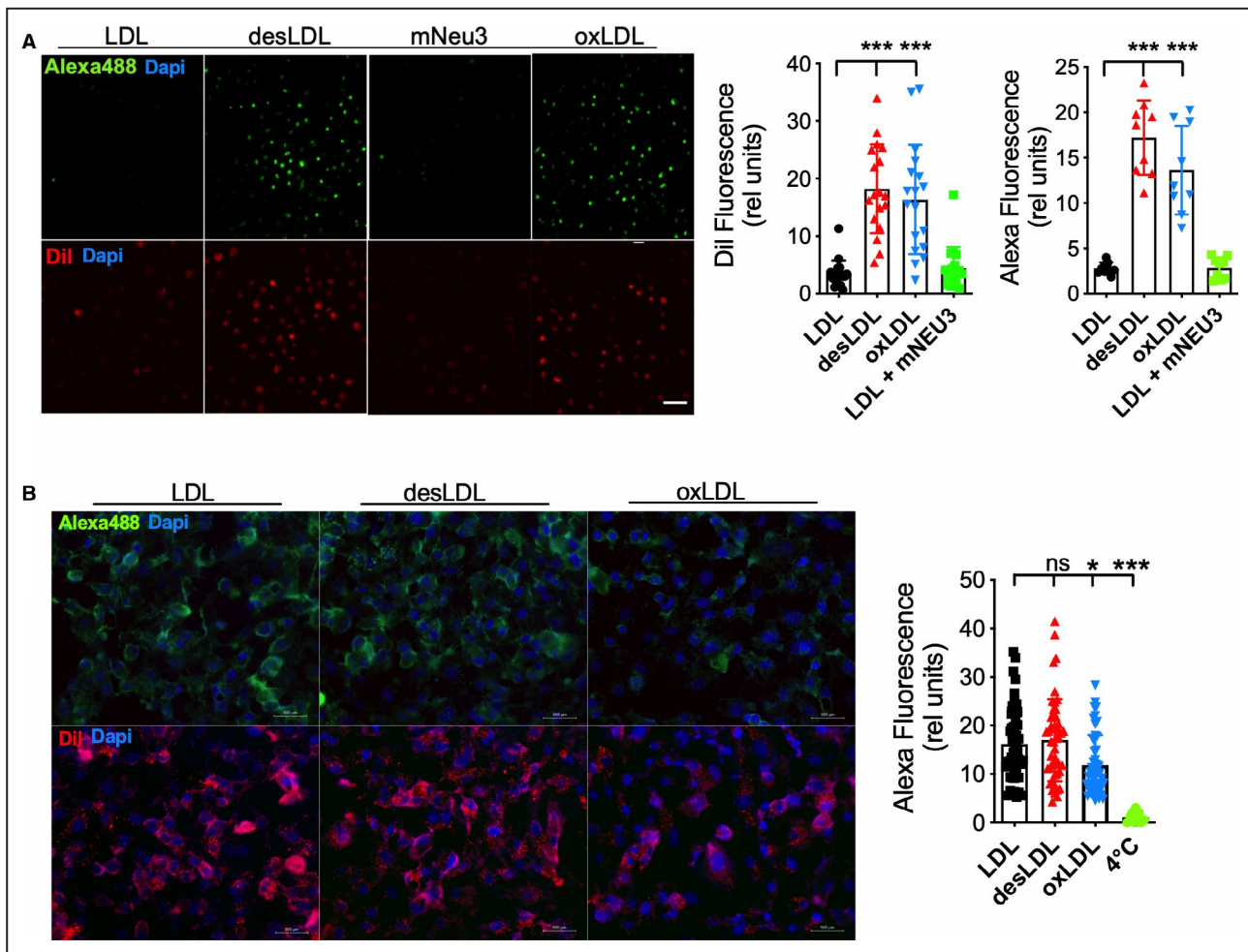


**Figure 2.** Desialylation increases low-density lipoprotein (LDL) uptake by cultured human macrophages but not the endocytosis by HepG2 cells.

**A**, Desialylation increases LDL uptake by cultured macrophages. Human peripheral blood mononuclear cell-derived macrophages, starved overnight in lipoprotein-deficient serum, were incubated with labeled native LDL, oxidized LDL (oxLDL), and LDL treated with human recombinant neuraminidase 3 (NEU3) (desialylated LDL [desLDL]) or enzymatically inactive mutant NEU3 (LDL+mNEU3-Tyr370Phe mutant [mNEU3]). After incubation, cells were washed, fixed, and analyzed by confocal microscopy. Panels show typical images of macrophages treated with Alexa 488-labeled or 3,3'-diiodoacetylindocarbocyanine (DiI)-labeled LDL, and bar graphs present fluorescence intensities of cells quantified with ImageJ software. Data show mean values $\pm$ SD of three independent experiments.  $***P<0.001$  compared with native LDL in 1-way ANOVA (Alexa-labeled LDL) or Kruskal-Wallis (DiI-labeled LDL) test, followed by the Dunn multiple comparisons test. **B**, Desialylation does not affect LDL uptake by cultured HepG2 cells. HepG2 cells were incubated with labeled LDL, desLDL, or oxLDL for 20 minutes at 37°C or 4°C and, after washing and fixation, were analyzed by fluorescent microscopy. Panels show typical images of HepG2 cells treated with Alexa 488-labeled or DiI-labeled LDL, and bar graph presents average Alexa 488 fluorescence intensities of cells quantified with ImageJ software. Plot shows mean values $\pm$ SD of 3 independent experiments.  $*P<0.05$  and  $***P<0.001$  compared with the uptake of LDL at 37°C in Kruskal-Wallis test, followed by the Dunn multiple comparisons test. Dapi indicates 4',6-diamidino-2-phenylindole; and rel, relative.

comparing  $>2$  groups. Two-way ANOVA, followed by Bonferroni post hoc test, was used for 2-factor analysis.  $P\leq 0.05$  was considered significant.

## RESULTS

### ApoB in Human LDL Is Desialylated in Vitro by NEU1 to NEU4

The major goal of our study was to test the hypothesis that endogenous neuraminidases present in

plasma, on the surface of hematopoietic cells, or in arterial endothelium contribute to the development of atherosclerosis by removing sialic acid residues from glycan chains of LDL glycoproteins and glycolipids. First, we studied if human neuraminidases can cleave sialic acid residues from ApoB in LDL in vitro. The LDLs isolated from healthy human subjects were treated with recombinant human NEU1, NEU2, NEU3, and NEU4 enzymes; and the structures of ApoB N-glycans, released by PNGase F endoglycosidase, were analyzed using ultraperformance LC-MS/MS



(Figure 1A, left panel). Treatment with neuraminidases caused drastic changes in the sialylation of the N-glycans: the levels of glycans with  $\geq 2$  sialic acids were reduced, and those of monosialylated or asialo glycans were generally increased (Figure 1A, right panel, and Tables S1 and S2). The structure of the glycan chains of ApoB in native and desialylated LDLs was further analyzed in detail by tandem mass spectroscopy. Sites containing N-linked glycans were identified by Proteinase K digestion of ApoB, followed by extraction of peptides and their analysis by LC-MS/MS. This analysis directly confirmed that sialic acid residues were removed from the complex glycan chains linked to asparagine residues 7, 956, 1350, 2752, 3074, 3309, 3331, 3868, and 4210, reducing the total sialylation of glycan chains from 96% to 36% (Figure 1B and Tables S3 and S4).

The LC-MS/MS results were confirmed by blotting with *Maackia amurensis* lectin-II lectin 2 to 4, specific for  $\alpha$ -2,3-linked Sia residues and *Sambucus nigra* lectin that binds preferentially to sialic acid attached to terminal galactose in  $\alpha$ -2,6 and, to a lesser degree,  $\alpha$ -2,3 linkage.<sup>31,32</sup> Incubation of LDLs with NEU1 to NEU4 resulted in drastically reduced lectin binding to ApoB (Figure 1C). Moreover, ApoB from LDLs treated with NEU1 to NEU4 but not from native LDL was recognized by peanut (*Arachis hypogaea*) agglutinin lectin, specific to carbohydrate sequence Gal- $\beta$ (1-3)-GalNAc, which typically underlies Sia residues (Figure 1C). More important, desialylation of ApoB did not occur in the presence of the pan-selective neuraminidase inhibitor, 2,3-didehydro-2-deoxy-N-acetyl-neuraminic acid (DANA; 1 mmol/L final concentration; Figure S1), or following incubation with the catalytically inactive NEU3-Tyr370Phe mutant<sup>33</sup> (data not shown).

### Desialylation of LDLs Increases Their Uptake by Cultured Human Monocyte-Derived Macrophages But Not by HepG2 Cells

To test whether desialylation of LDLs could affect their uptake by macrophages, we treated cultured human blood monocyte-derived macrophages with fluorescently labeled native LDL, desialylated LDL (desLDL; desialylated by NEU3), or oxidized LDL (oxLDL). To analyze simultaneously the uptake of the LDL particles and cholesterol, we used 2 types of labels, 488 or 594 Alexa Fluor, which covalently modifies the ApoB molecule, and 3,3'-dioctadecylindocarbocyanine (1,1'-dioctadecyl-3,3,3',3'-tetramethylindocarbocyanine perchlorate), which incorporates into the LDL lipid core. Incubation of human macrophages with desLDL resulted in significantly higher accumulation of both Alexa and 3,3'-dioctadecylindocarbocyanine labels, compared with cells incubated with similarly

labeled native LDL or LDL treated with the enzymatically inactive NEU3-Tyr370Phe mutant (Figure 2A). This result is consistent as a suggestion that removal of Sia from ApoB by neuraminidases dramatically increases LDL uptake by cultured macrophages. Moreover, desLDLs were engulfed at a rate similar to that of oxLDL (Figure 2A), suggesting that both modifications have similar effects on LDL uptake by macrophages.

To analyze if desialylation alters the ability of LDL to bind the hepatocyte LDL receptor (LDLR), we tested the uptake of native LDL and desLDL by cultured human hepatocellular carcinoma cells (HepG2). Similarly to primary hepatocytes, HepG2 cells express high levels of LDLR and are routinely used to study the LDL uptake by the LDLR-mediated pathway. Cultured HepG2 cells were incubated in the presence of LDL and desLDL labeled with Alexa Fluor or 3,3'-dioctadecylindocarbocyanine, and the uptake of the dye into the cells was quantified as above for macrophages. Native and desialylated LDLs were taken up by cultured HepG2 cells at a similar rate (Figure 2B), suggesting that desialylation of LDLs did not alter their binding to LDLRs. In contrast, oxLDL showed a 40% reduced uptake rate, consistent with previously reported data.<sup>34,35</sup>

### Macrophages Incorporate desLDL via an ASGR1-Dependent Pathway

To study if scavenger receptors, such as CD68, CD36, or scavenger receptor class B type 1, implicated in the incorporation of oxLDL, are also involved in endocytosis of desLDL, we analyzed uptake of labeled desLDL by macrophages in the presence of 5-, 10-, or 20-fold excess of unlabeled desLDL or oxLDL (Figure 3A). The uptake of labeled desLDL was completely blocked by an excess of unlabeled desLDL, but only partially inhibited by an excess of unlabeled oxLDL, suggesting an existence of a separate endocytic pathway for desLDL.

Because desialylation likely exposes a subterminal Gal-GlcNAc disaccharide in the ApoB glycans, we hypothesized that endocytic pathways specific for desLDL may involve Gal-GlcNAc-specific lectins, such as ASGRs (ASGR1 and ASGR2; collectively named Ashwell-Morell receptor), or galectin-3. Galectin-3 is abundant in monocytic cells and macrophages and plays an important role in their activation and phagocytosis.<sup>36</sup> The expression of ASGRs is thought to be mainly restricted to the liver cells, including parenchymal hepatocytes and liver macrophages<sup>37</sup>; however, ASGR1 expression has been also reported in monocytes. More important, the receptor has been proposed to participate in clearance of aged LDL and chylomicron remnants.<sup>38,39</sup>

To explore the hypothesis that desLDLs are endocytosed by human macrophages via galactose-specific lectin receptors, we studied if this process can be inhibited by Gal-containing disaccharides. These compounds (see supplemental materials for description of synthesis) exhibit specific inhibition of Gal-specific lectins, such as galectin-3, with  $K_i$  values in the low micromolar range. The uptake of desLDL was almost completely inhibited in the presence of 500  $\mu\text{mol/L}$  2-naphthyl 3'-*O*-sulfo- $\beta$ -D-lactopyranoside (Figure 3B) or 500  $\mu\text{mol/L}$  2-naphthyl 3'-*O*-sulfo-1-thio- $\beta$ -D-lactopyranoside (not shown), consistent with the suggestion that Gal/GlcNAc-specific lectins are involved in their incorporation. Besides, the presence of Alexa-labeled desLDL (but not LDL) in the culture medium of macrophages significantly increased cellular uptake of fluorescein isothiocyanate-labeled galectin-3C, the recombinant soluble lectin domain of human galectin-3 protein<sup>40</sup> (Figure 3B). Galectin-3C colocalized inside the macrophages with Alexa, suggesting that this protein could be endocytosed by the cells as a complex with desLDL.

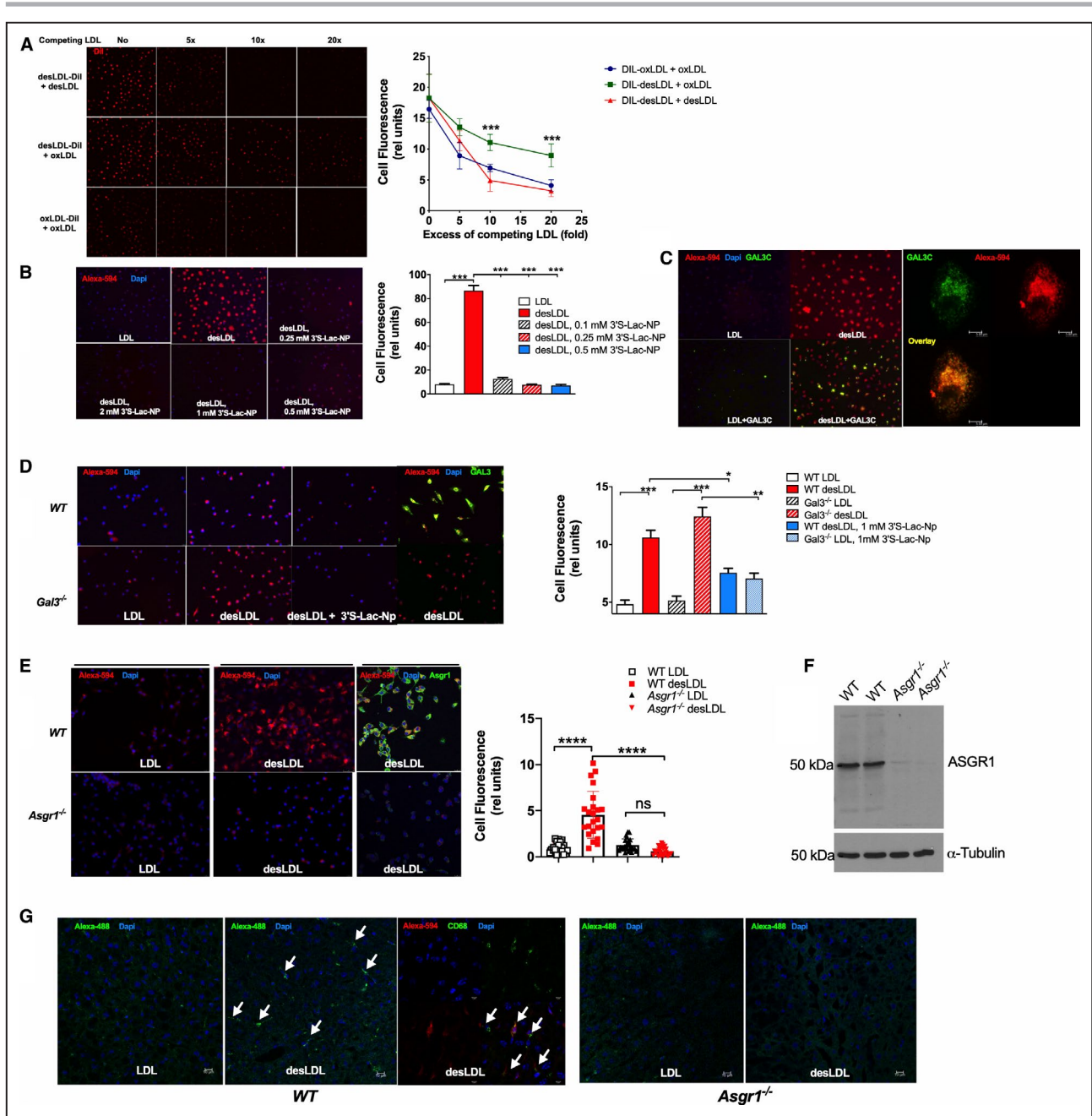
To test if galectin-3 is directly involved in the uptake of desialylated LDL, we studied the uptake of Alexa-labeled desLDL by cultured BMDMs from *Gal3*

knockout mice (B6.Cg-Lgals3tm1Poi/J).<sup>41</sup> BMDMs from WT and *Gal3* knockout mice were loaded with Alexa 488-labeled human LDL or desLDL, as has been previously done for human peripheral blood mononuclear cell-derived macrophages in the absence or presence of 2-naphthyl 3'-*O*-sulfo- $\beta$ -D-lactopyranoside. As with the human peripheral blood mononuclear cell-derived macrophages, WT mouse BMDMs demonstrate much higher rates of desLDL uptake compared with native LDL (Figure 3D). However, no differences in the desLDL incorporation were observed between galectin-3-positive or galectin-3-negative cells, indicating that this protein is not involved in desLDL uptake. In both WT and galectin-3 knockout cells, 2-naphthyl 3'-*O*-sulfo- $\beta$ -D-lactopyranoside showed equal efficacy in blocking the incorporation of desLDL, suggesting that the drug's target is not galectin-3.

Previously, ASGR1 has been shown to play a leading role in the removal of aged secreted proteins and hematopoietic cells from circulation.<sup>42</sup> In this pathway, the N-glycans of the secreted and cell surface proteins are desialylated by circulating NEU1 and NEU3, and, as a result, exposed Gal-GlcNAc residues are recognized by ASGR1 on hepatocytes and spleen macrophages and endocytosed.<sup>42</sup> To test if ASGR1 is also involved in the rapid uptake of

**Figure 3. Macrophages incorporate desialylated low-density lipoprotein (desLDL) via asialoglycoprotein receptor (ASGR) 1 pathway.**

**A**, Oxidized low-density lipoproteins (oxLDLs) only partially block the uptake of desLDLs by macrophages. Cultured macrophages were loaded with 3,3'-dioctadecylindocarbocyanine (DiI)-labeled desLDLs or oxLDLs in the presence of 5-, 10-, or 20-fold excess of unlabeled oxLDLs or desLDLs. Cells were washed, fixed, and analyzed by fluorescence microscopy. Panels show representative images of 3 independent experiments. Graph shows mean values $\pm$ SD of relative fluorescence intensities of cells measured by ImageJ software.  $**P<0.01$  in 2-way ANOVA with Bonferroni post hoc test. **B**, The uptake of desLDLs by macrophages is blocked by a galectin inhibitor, 2-naphthyl 3'-*O*-sulfo- $\beta$ -D-lactopyranoside (3'S-Lac-NP). Cultured macrophages were incubated with Alexa 594-labeled low-density lipoprotein (LDL) or desLDL in the absence or presence of 2 mmol/L 3'S-Lac-NP, washed, fixed, and analyzed by fluorescence microscopy. Panels show representative images of 3 independent experiments. Graph shows mean values $\pm$ SD of relative fluorescence intensities of the cells measured by ImageJ software.  $*P<0.05$ ,  $**P<0.01$ , and  $***P<0.001$  in 1-way ANOVA test, followed by the Tukey multiple comparisons test. **C**, Recombinant soluble Gal-binding galectin-3 (GAL3) domain, GAL3C, is endocytosed by macrophages in the presence of desLDL, but not of native LDL. Cultured macrophages were incubated with Alexa 594-labeled LDL or desLDL in the presence of fluorescein isothiocyanate (FITC)-labeled GAL3C, washed, fixed, and studied by confocal microscopy. Panels show representative images of 3 independent experiments. Enlarged cell image shows colocalization of FITC-GAL3C and Alexa 594-desLDL. **D**, Cultured macrophages derived from bone marrow of wild-type (WT) and *Gal3* knockout (KO) C57Bl6 mice show similar uptake of desLDL, which can be inhibited by 3'S-Lac-NP. BMDMs from WT and homozygous *Gal3*<sup>-/-</sup> mice were incubated with Alexa 594-labeled LDL or desLDL (red) in the absence or presence of 2 mmol/L 3'S-Lac-Np, washed, fixed, stained with monoclonal antibodies against GAL3 protein (green), and analyzed by fluorescence microscopy. Panels show representative images of 3 independent experiments. Graph shows mean values $\pm$ SD of relative fluorescence intensities of the cells measured by ImageJ software.  $**P<0.01$  in 1-way ANOVA test, followed by the Tukey multiple comparisons test. **E**, Cultured macrophages derived from bone marrow of *Asgr1* KO mice show impaired uptake of desLDL. Bone marrow-derived macrophages (BMDMs) from WT and homozygous *Asgr1*<sup>-/-</sup> mice were incubated with Alexa 594-labeled LDL or desLDL (red), washed, fixed, stained with monoclonal antibodies against *Asgr1* protein (green), and analyzed by fluorescence microscopy. Panels show representative images of 3 independent experiments. Graph shows mean values $\pm$ SD of relative fluorescence intensities of the cells measured by ImageJ software.  $****P<0.001$  in ANOVA test, followed by the Tukey multiple comparisons test. **F**, *Asgr1* immunoreactive band is present in BMDMs from WT but not from *Asgr1*<sup>-/-</sup> mice. Proteins (40  $\mu\text{g}$ ) of total cell lysates from *Asgr1*<sup>-/-</sup> and WT BMDMs were resolved on an 8% gradient SDS-PAGE gel, transferred to nitrocellulose membranes, and hybridized with anti-ASGPR1 antibody (NBP1-60150; Novus Biologicals; 1:100) and anti- $\alpha$ -tubulin antibody (12G10; Hybridoma Bank; 1:4000). Panel shows a representative image of 3 independent experiments. **G**, Liver macrophages of *Asgr1* KO mice show impaired uptake of desLDL. Accumulation of native LDL and desLDL, labeled with Alexa-488 (green) or Alexa-594 (red), in the livers of WT and *Asgr1*<sup>-/-</sup> mice, was studied 8 hours after systemic injection at a dose of 200  $\mu\text{g}$ . Sectioned livers were analyzed by fluorescent confocal microscopy. Panels show typical images of mice treated with labeled LDL or desLDL. Scattered cells, strongly positive for Alexa, with a shape and size characteristic of liver macrophages/Kupffer cells and positive for cluster of differentiation 68 (CD68) (arrowheads) were present only in the livers of WT mice treated with desLDL. Dapi indicates 4',6-diamidino-2-phenylindole.



desLDL by macrophages, we established cultures of BMDM macrophages from WT and *Asgr1*<sup>-/-</sup> mice and treated them with Alexa 594–labeled human LDL and desLDL, as described above. The cells were then washed, fixed, stained with monoclonal antibodies against ASGR1 protein, and analyzed by fluorescence microscopy. Our data (Figure 3E) demonstrate that, in contrast with BMDMs from WT mice, macrophages from *Asgr1*<sup>-/-</sup> mice show a negligible uptake of desLDL (Figure 3E). The cells from WT mice, but not from *Asgr1*<sup>-/-</sup>, showed strong reactivity toward anti-ASGR1 antibody (Figure 3E). In similar manner, Western blot analysis of WT BMDM

protein lysates demonstrated a presence of a 50-kDa ASGR1 immunoreactive protein band absent in *Asgr1*<sup>-/-</sup> cells, confirming that the ASGR1 receptor is expressed not only in liver Kupffer cells but also in BMDMs (Figure 3F). Similar results were obtained for the inflammatory peritoneal or splenocyte-derived *Asgr1*<sup>-/-</sup> macrophages (data not shown). We further injected Alexa-labeled desLDL and LDL into the tail vein of WT C57Bl/6J and *Asgr1*<sup>-/-</sup> 16-week-old mice (200  $\mu$ g/animal) and 8 hours after analyzed their fixed liver tissues by fluorescence confocal microscopy. In the livers of WT mice injected with desLDL, we detected scattered cells strongly positive for Alexa

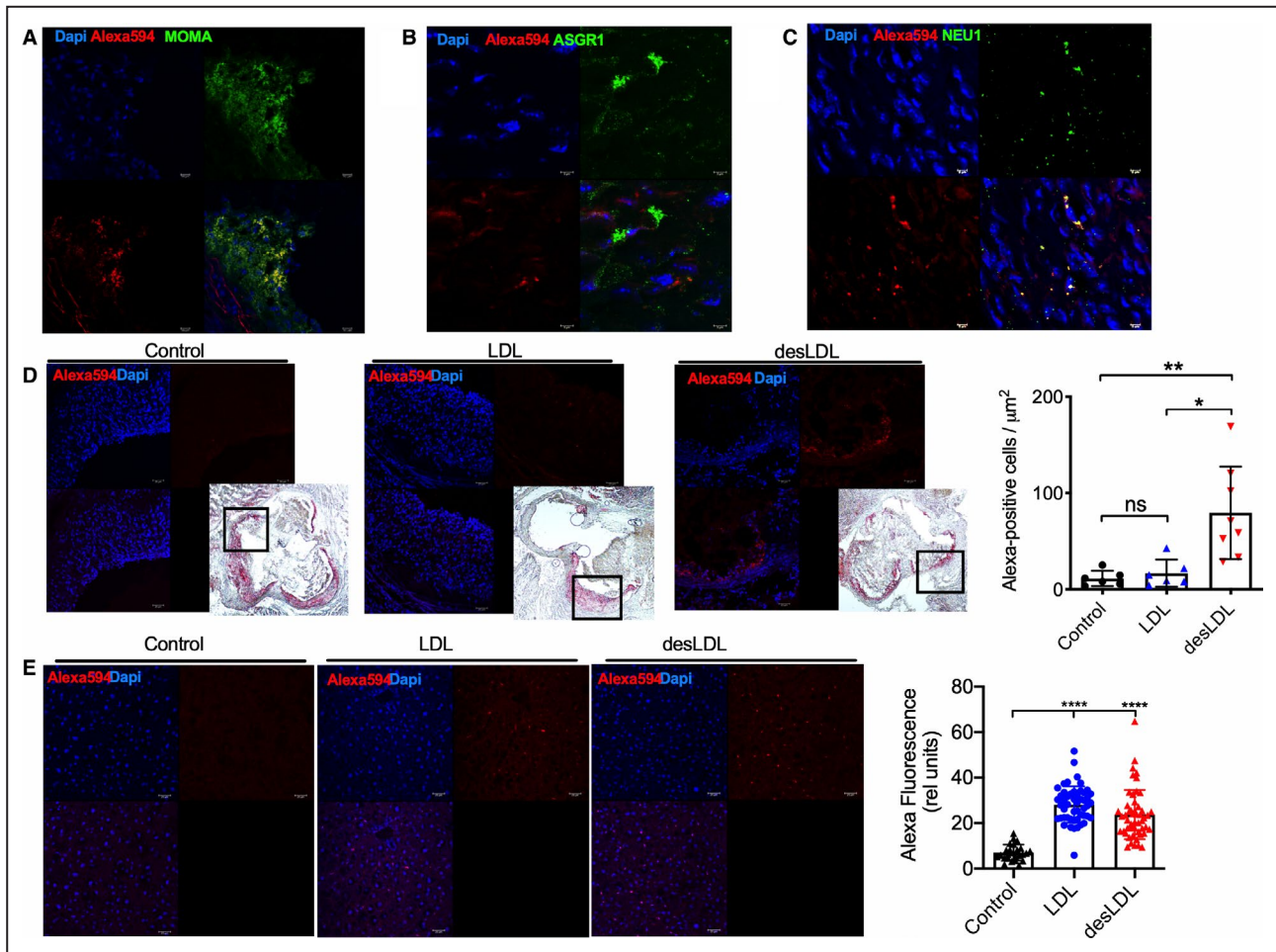


**Figure 4. Desialylation increases low-density lipoprotein (LDL) uptake by macrophages in atherosclerotic aortic root lesions but not by liver hepatocytes.**

**A** through **D**, Accumulation of native LDL and desialylated LDL (desLDL) in the aortic root lesions of 16-week-old *Apoe*<sup>-/-</sup> mice was studied 6 hours after systemic injection of 200  $\mu\text{g}$  of labeled LDL or desLDL. Aortic root sections were stained with monoclonal anti-macrophage antibody (MOMA-2) (**A**), polyclonal rabbit antibody against ASGR1 (**B**), or monoclonal rabbit antibody against neuraminidase 1 (NEU1) (**C**). **D**, Alexa 594 fluorescence in root sections was analyzed by fluorescent confocal microscopy. Panels show typical images of aortic root from untreated mice and those treated with Alexa 594-labeled LDL or desLDL. Bar graphs present average fluorescence intensities of aorta wall quantified with ImageJ software. Plots show mean values  $\pm$  SD obtained with 6 untreated mice and 6 LDL-treated and 8 desLDL-treated male and female mice. \* $P < 0.05$  and \*\* $P < 0.01$  compared with untreated and LDL-treated mice in Kruskal-Wallis test, followed by the Dunn multiple comparisons test. **E**, Desialylation does not affect LDL uptake by liver hepatocytes. Accumulation of native LDL and desLDL in the livers of mice was studied 6 hours after systemic injection of 200  $\mu\text{g}$  of labeled LDL. Sectioned livers were analyzed by fluorescent confocal microscopy. Relative fluorescence intensities were measured by ImageJ software. Panels show typical images of mice treated with Alexa 488-labeled LDL or desLDL. Graphs present fluorescence intensities of hepatocytes (individual and mean values  $\pm$  SD, measured in 50 cells from 4 mice per group). \*\*\*\* $P < 0.0001$  compared with untreated mice in Kruskal-Wallis test, followed by the Dunn multiple comparisons test. ASGR indicates asialoglycoprotein receptor; and Dapi, 4',6-diamidino-2-phenylindole.

with a shape and size characteristic of liver macrophages/Kupffer cells and stained with antibodies against the macrophage marker CD68 (Figure 3G). Alexa-positive/CD68-positive cells were not present in the livers of WT mice injected with labeled native LDL or in the livers of *Asgr1*<sup>-/-</sup> mice injected with both LDL and desLDL (Figure 3G). Together, these data are consistent with the hypothesis that the uptake of desLDL by macrophages is mediated by ASGR1.

### Desialylation Increases LDL Incorporation Into Macrophages of the Atherosclerotic Lesions in Mouse Aortic Root

We further studied if desialylation increased LDL uptake by the macrophages of the lesions in the aortic root in the mouse model of atherosclerosis. Sixteen-week-old female *Apoe*<sup>-/-</sup> mice, a commonly used spontaneous murine model of atherosclerosis,<sup>43</sup> were injected via the tail vein with 200  $\mu\text{g}$  of native LDL or

desLDL fluorescently labeled with Alexa 594 or 488. Eight hours after the injection, mice were euthanized, and their hearts and livers were collected and analyzed by confocal fluorescent microscopy for the presence of the label in the aortic root (Figure 4A through 4D) and liver (Figure 4E).

In the sections of the aortic root of mice injected with Alexa 594–labeled desLDL, the label mainly accumulated in the lesion areas positively stained with monoclonal anti–monocyte+macrophage antibody (Figure 4A). The Alexa 594–loaded cells were also highly positive for the expression of ASGR1 protein (Figure 4B) and NEU1 (Figure 4C). The quantification of the fluorescence intensity with ImageJ software demonstrated that the levels of Alexa 594 in the macrophages of the aortic lesion were significantly higher when mice were injected with desLDL compared with those injected with native LDL (Figure 4D). These results are consistent with the suggestion that desLDLs are incorporated by macrophages in the lesion at a higher rate than LDLs. On the other hand, fluorescence intensities of liver hepatocytes of mice injected with Alexa-labeled desLDL and LDL were not different, consistent with similar uptake of LDL and desLDL observed in cultured HepG2 cells (Figure 4E).

### Early Stages of Atherosclerosis Are Delayed in Gene-Targeted NEU1- and NEU3-Deficient Mice

To evaluate whether neuraminidases play a role in atheroma progression *in vivo*, we performed genetic inactivation of individual neuraminidases in female *ApoE*<sup>-/-</sup> mice.<sup>43</sup> Compared with WT C57Bl/6J mice, *ApoE*<sup>-/-</sup> mice have significantly increased levels of total cholesterol and LDL cholesterol in blood,<sup>44</sup> even when they are fed a regular diet. At ≈15 weeks of life, female *ApoE*<sup>-/-</sup> mice develop intermediate aortic lesions containing both foam and smooth muscle cells.<sup>45</sup>

Three mouse strains were generated, all in the same C57Bl/6J background. *ApoE*<sup>-/-</sup> *Neu3*<sup>-/-</sup> and *ApoE*<sup>-/-</sup> *Neu4*<sup>-/-</sup> double-knockout mice were produced by crossing homozygous *ApoE*<sup>-/-</sup> mice with previously described homozygous *Neu3*<sup>-/-</sup> and *Neu4*<sup>-/-</sup> mice, respectively.<sup>21,22</sup> To produce NEU1-deficient strain, we crossed *ApoE*<sup>-/-</sup> mice with previously described cathepsin A hypomorph mice (*CathA*<sup>S190A-Neo</sup>).<sup>20</sup> These mice have an ≈90% reduction in NEU1 activity in tissues,<sup>20</sup> but they do not develop a rapidly progressing multisystemic disease occurring in constitutive *Neu1* knockout models because of the lysosomal storage of sialoglycoconjugates.<sup>46</sup> Available in our laboratory, constitutive *Neu1* knockout mice develop lethargy, reduced motor

coordination, myoclonus, reduced weight gain (≈30% of WT), increased circulating levels of proinflammatory cytokines, and urinary retention by 14 weeks of age, which makes them unsuitable for long-term physiological studies (I.-H. Kho and E. Demina, unpublished data, 2020). In contrast, *CathA*<sup>S190A-Neo</sup> as well as *Neu3* and *Neu4* knockout mice are fertile and display normal development, with the increase of BW over age, similar to that of normal mice.<sup>20-22</sup>

To analyze if neuraminidases are involved in the initial stage of atherosclerosis, mice were euthanized at 16 weeks (the age when they show intermediate foam cell lesions<sup>45</sup>), and lipid depositions were analyzed in the aortic root sections. Analysis of *ApoE*<sup>-/-</sup> *CathA*<sup>S190A-Neo</sup> and *ApoE*<sup>-/-</sup> *Neu3*<sup>-/-</sup> mice showed fatty streak lesions with a significantly smaller average area than in control *ApoE*<sup>-/-</sup> female mice: 173 000±13 300 μm<sup>2</sup> for *ApoE*<sup>-/-</sup> versus 122 000±8000 μm<sup>2</sup> for *ApoE*<sup>-/-</sup> *CathA*<sup>S190A-Neo</sup> and 118 000±19 200 μm<sup>2</sup> for *ApoE*<sup>-/-</sup> *Neu3*<sup>-/-</sup> mice (Figure 5A). Conversely, the mean sizes of atherosclerotic lesions for *ApoE*<sup>-/-</sup> *Neu4*<sup>-/-</sup> and *ApoE*<sup>-/-</sup> mice were similar. In addition to aortic sinus, we also analyzed the area of Sudan IV–stained fatty streaks at the aorta face of 20-week-old *ApoE*<sup>-/-</sup> *CathA*<sup>S190A-Neo</sup> mice and found that lesion size was also significantly reduced in these mice compared with control *ApoE*<sup>-/-</sup> mice (Figure S2). Collectively, these results clearly demonstrated that deficiency of NEU1 or NEU3, but not of NEU4, is associated with a dramatic reduction of the lesion size in *ApoE*<sup>-/-</sup> mice.

Because previous reports have demonstrated that NEU1 (and potentially NEU3 and NEU4) can regulate inflammatory response, including cytokine production and migration of immune cells,<sup>47,48</sup> we analyzed infiltration of T cells and macrophages in atherosclerotic lesions by immunohistochemistry using monoclonal anti–monocyte+macrophage antibody or goat polyclonal anti-mouse CD3 antibody. We found significantly reduced anti–monocyte+macrophage antibody–positive areas for the atherosclerotic lesions from NEU1-deficient *ApoE*<sup>-/-</sup> *CathA*<sup>S190A-Neo</sup> compared with *ApoE*<sup>-/-</sup> mice, consistent with reduced infiltration of macrophages (Figure 5B). Anti–monocyte+macrophage antibody–positive areas of the lesions were similar between *ApoE*<sup>-/-</sup> *Neu3*<sup>-/-</sup>, *ApoE*<sup>-/-</sup> *Neu4*<sup>-/-</sup>, and *ApoE*<sup>-/-</sup> animals, suggesting that multiple mechanisms may underlie reduced formation of fatty streaks in NEU1-deficient and NEU3-deficient mice. No significant differences were observed in CD3 staining of the lesions for any strain (data not shown).

The analysis of mouse plasma did not reveal significant differences in the levels of total cholesterol, LDL cholesterol, HDL cholesterol, or triglycerides between *ApoE*<sup>-/-</sup> and *ApoE*<sup>-/-</sup> *CathA*<sup>S190A-Neo</sup> mice (Figure 5C), suggesting that the decrease in the size

of the atherosclerotic lesions in NEU1-deficient mice was not associated with changes in plasma cholesterol levels. Total, HDL cholesterol, and LDL cholesterol levels were slightly reduced in *Apoe*<sup>-/-</sup> *Neu3*<sup>-/-</sup> mice compared with the *Apoe*<sup>-/-</sup> *Neu4*<sup>-/-</sup> mice. The mechanisms underlying these data and their physiological importance remain to be studied; however, we did not detect any correlation between the LDL/total cholesterol levels and the size of fatty streaks in the sinus of the individual *Apoe*<sup>-/-</sup> *Neu3*<sup>-/-</sup> mice (Figure S3). We, therefore, believe that the changes in total cholesterol and LDL cholesterol levels were not responsible for the reduction of atherosclerosis lesions in the NEU3-deficient strain.

To further test whether deficiencies of individual neuraminidases caused changes in sialylation of glycolipids present in lipoproteins, we analyzed mouse plasma, where LDLs act as carriers for gangliosides.<sup>49</sup> The major ganglioside observed in all samples was GM2, containing a Neu5Gc residue (3–3.5 µg/mL), which was in accordance with previously reported data.<sup>50</sup> Other detected minor gangliosides were GM1, GA2, GM3 containing Neu5Gc, GM3, and LacCer. The ganglioside composition was similar for *Apoe*<sup>-/-</sup>, *Apoe*<sup>-/-</sup> *Neu3*<sup>-/-</sup>, and *Apoe*<sup>-/-</sup> *Neu4*<sup>-/-</sup> mice, but the serum from *Apoe*<sup>-/-</sup> *CathA*<sup>S190A-Neo</sup> mice showed reduced levels of both the major Neu5Gc-GM2 and minor GM1, GA2, and GM3 gangliosides (Figure 5D). Because our previous work provided evidence against a direct involvement

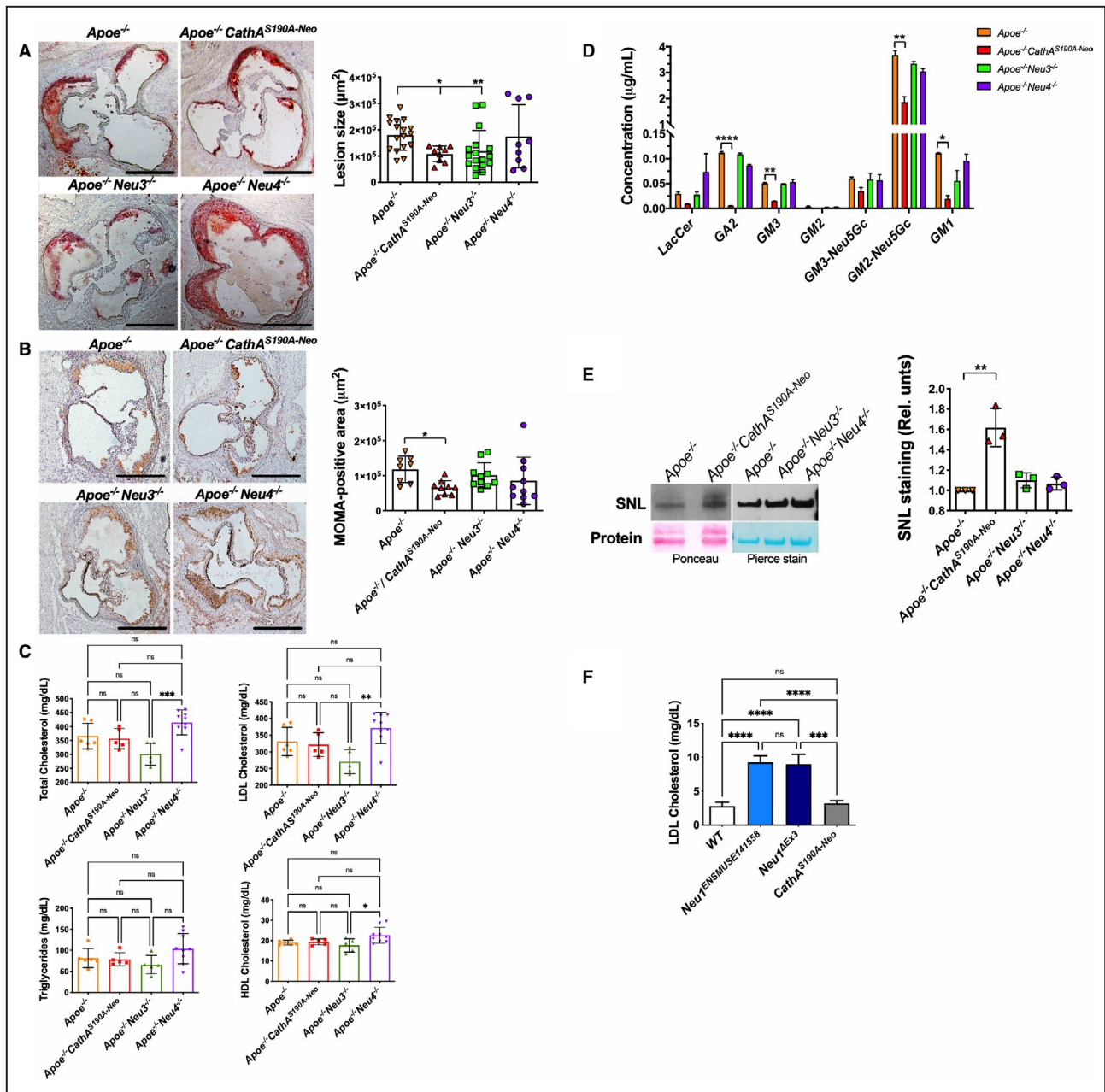
of NEU1 in ganglioside processing,<sup>24</sup> we speculate that these changes in *Apoe*<sup>-/-</sup> *CathA*<sup>S190A-Neo</sup> mice are related to secondary increase in the expression of NEU3 and NEU4 that may occur to compensate for NEU1 deficiency.<sup>24</sup> Nevertheless, the major plasma ganglioside, Neu5Gc-GM2, although reduced by ~30%, remained in high abundance in the NEU1-deficient mice. This, together with the absence of changes in the other mutants, suggested that variations in plasma ganglioside composition alone do not explain reduced lesion formation.

To test whether the delay of atherosclerosis in the NEU1-deficient mice is associated with increased ApoB sialylation, we analyzed LDLs purified from the pooled blood of *Apoe*<sup>-/-</sup>, *Apoe*<sup>-/-</sup> *Neu3*<sup>-/-</sup>, *Apoe*<sup>-/-</sup> *Neu4*<sup>-/-</sup>, and *Apoe*<sup>-/-</sup> *CathA*<sup>S190A-Neo</sup> mice by *Sambucus nigra* lectin blot. Quantification of the intensity of *Sambucus nigra* lectin-stained ApoB bands showed that ApoB sialylation in the blood from *Apoe*<sup>-/-</sup> *CathA*<sup>S190A-Neo</sup>, but not from *Apoe*<sup>-/-</sup> *Neu3*<sup>-/-</sup> and *Apoe*<sup>-/-</sup> *Neu4*<sup>-/-</sup>, mice was significantly increased compared with that in *Apoe*<sup>-/-</sup> mice (Figure 5E).

To test the hypothesis that deficiency of NEU1 causes increased sialylation and reduced uptake of LDL, we measured LDL cholesterol in the blood plasma of C57Bl6 mice and in 3 strains of NEU1-deficient mice: *CathA*<sup>S190A-Neo</sup> mice and 2 constitutive NEU1 knockout strains. The previously described *Neu1*<sup>ENSMUSE141558</sup> mouse strain was generated by microinjection in C57BL6J blastocysts of the embryonic stem cells, with

**Figure 5. Early stages of atherosclerosis are delayed in *Apoe*<sup>-/-</sup> mice with neuraminidase 1 (NEU1) and neuraminidase 3 (NEU3) deficiency.**

**A**, Size of fatty streaks is reduced in the aortic root of *Apoe*<sup>-/-</sup> mice deficient in NEU1 and NEU3. Female *Apoe*<sup>-/-</sup> mice (n=17) and *Apoe*<sup>-/-</sup> mice deficient in NEU1 (n=9), NEU3 (n=17), or neuraminidase 4 (NEU4) (n=9) were euthanized at the age of 16 weeks. Atherosclerosis was analyzed by staining fatty streaks in the aortic root sections with Red Oil O. Microphotographs show representative images of aortic root sections. Bar=500 µm. The graph shows atherosclerotic lesion size in the aortic roots (µm<sup>2</sup>) measured by ImageJ software. \**P*<0.05 and \*\**P*<0.01 compared with *Apoe*<sup>-/-</sup> mice in Kruskal-Wallis test, followed by the Dunn multiple comparisons test. **B**, Macrophage infiltration is reduced in atherosclerotic aortic root lesions of *Apoe*<sup>-/-</sup> mice deficient in NEU1. Macrophage infiltration was studied in 16-week-old *Apoe*<sup>-/-</sup> (n=8), *Apoe*<sup>-/-</sup> *CathA*<sup>S190A-Neo</sup> (n=9), *Apoe*<sup>-/-</sup> *Neu3*<sup>-/-</sup> (n=10), and *Apoe*<sup>-/-</sup> *Neu4*<sup>-/-</sup> (n=10) mice. Panels show representative photomicrographs of aortic root sections stained with anti-macrophage antibody (MOMA-2) antibodies. Bar=50 µm. The graph shows areas of MOMA-2-positive area (µm<sup>2</sup>) measured by ImageJ software. At least 4 sections per mouse were examined. Data represent mean±SD. \**P*<0.05 in Kruskal-Wallis test, followed by the Dunn multiple comparisons test. **C**, Lipid plasma composition of 16-week-old female *Apoe*<sup>-/-</sup>, *Apoe*<sup>-/-</sup> *Neu4*<sup>-/-</sup>, *Apoe*<sup>-/-</sup> *Neu3*<sup>-/-</sup>, and *Apoe*<sup>-/-</sup> *CathA*<sup>S190A-Neo</sup> mice. Total cholesterol, triglyceride, high-density lipoprotein (HDL) cholesterol, and low-density lipoprotein (LDL) cholesterol levels were measured in plasma samples. Data represent mean±SD. \**P*<0.05, \*\**P*<0.01, and \*\*\**P*<0.001 in 1-way ANOVA test, followed by the Tukey multiple comparisons test. **D**, Ganglioside composition of plasma from 16-week-old female *Apoe*<sup>-/-</sup>, *Apoe*<sup>-/-</sup> *Neu4*<sup>-/-</sup>, *Apoe*<sup>-/-</sup> *Neu3*<sup>-/-</sup>, and *Apoe*<sup>-/-</sup> *CathA*<sup>S190A-Neo</sup> mice. Values show mean±SD (n=3). The major glycan observed in all samples is GM2 containing a Neu5Gc residue (3–3.5 µg/mL).<sup>50</sup> Other minor gangliosides are GM1, GA2, GM3 containing Neu5Gc, GM3, and LacCer. \**P*<0.05, \*\**P*<0.01, and \*\*\*\**P*<0.0001 compared with *Apoe*<sup>-/-</sup> mice in Kruskal-Wallis test, followed by the Dunn multiple comparisons test. **E**, Increased sialylation of LDL apolipoprotein B 100 (ApoB) in the blood of *CathA*<sup>S190A-Neo</sup> mice. Blood was collected by cardiac puncture into EDTA-coated tubes from *Apoe*<sup>-/-</sup>, *Apoe*<sup>-/-</sup> *Neu4*<sup>-/-</sup>, *Apoe*<sup>-/-</sup> *Neu3*<sup>-/-</sup>, and *Apoe*<sup>-/-</sup> *CathA*<sup>S190A-Neo</sup> female 16-week-old mice (7–10 animals/group). For each group, LDL (d=1.019 to 1.063 g/mL) was isolated from 4 mL of pooled plasma by sequential density gradient ultracentrifugation. Sialylation of the ApoB was analyzed by lectin blotting using biotinylated *Sambucus nigra* lectin (SNL). The panel shows images of representative blots and corresponding membranes stained for protein by Ponceau S or Pierce Reversible Protein Stain. The graph shows results of quantification (SNL staining normalized for protein band intensity; mean values±SD) performed for 3 individual blots by ImageJ software. \*\**P*<0.01 compared with wild type (WT) in Kruskal-Wallis test, followed by the Dunn multiple comparisons test. **F**, LDL levels are increased in the plasma of Neu1 knockout (KO) mice. LDL cholesterol levels were measured in plasma samples of 8-week-old C57Bl6J (WT) and NEU1-deficient *CathA*<sup>S190A-Neo</sup> mice, as well as Neu1 KO *Neu1*<sup>ENSMUSE141558</sup> and *Neu1*<sup>ΔEx3</sup> mice. Data represent mean±SD. \*\*\*\**P*<0.001 compared with WT mice in 1-way ANOVA test, followed by the Tukey multiple comparisons test.



targeted disruption of the *Neu1* gene generated by the European Conditional Mouse Mutagenesis Program consortia. The targeted *Neu1*<sup>ENSMUSE141558</sup> allele contains *LacZ/BactPNeo* cassette inserted into the intron 2 of the mouse *Neu1* gene, resulting in the expression of a fusion protein containing the mouse NEU1 amino acid sequence encoded by exons 1 to 2 and followed by the bacterial β-galactosidase encoded by the *LacZ* gene.<sup>24</sup> The second strain, *Neu1*<sup>ΔEx3</sup>, was obtained by crossing the *Neu1*<sup>ENSMUSE141558</sup> mouse with C57Bl6J mice constitutively expressing Cre recombinase that resulted in removal of the entire exon 3 from the *Neu1* gene. In both strains, intact *Neu1* mRNA and NEU1 activity levels in tissues were below detectable levels (Figure S4).

As expected, LDL levels in the WT C57Bl6J mice were at or below the detection level (3 mg/dL) (Figure 5F). The *CathA*<sup>S190A-Neo</sup> mice also showed negligible LDL levels, but in both constitutive *Neu1* knockout strains, LDL levels were increased ~3-fold (Figure 5F). These results not only independently confirmed our hypothesis about the NEU1-driven uptake of LDL but also established the safe threshold for inhibition of NEU1 in circulation. The reduction of the residual NEU1 activity in the *CathA*<sup>S190A-Neo</sup> mice to 10% to 20% significantly delayed the atherogenesis without interfering with the LDL level or causing lysosomal storage of sialoglycoconjugates in tissues.<sup>20</sup>

**Table 1. In Vitro Activity of NEU1 and NEU3 Inhibitors Used in This Study**

Compound*	IC <sub>50</sub> , μmol/L†	Selectivity	K <sub>i</sub> , μmol/L‡			
			NEU1	NEU2	NEU3	NEU4
DANA	8/8	NEU3/NEU4; 4x	12±1	25±4	1.6±0.3	5.8±0.6
CG17701	0.7/0.5	NEU3/NEU4; 45x	ND	48±9	0.28±0.04	0.26±0.04
CG22601	0.6	NEU3; 10x	ND	17±4	0.32±0.04	5±1
CG14601	0.99	NEU1; 33x	0.24±0.03	ND	ND	ND
C9-BA-DANA	3	NEU1; 32x	0.83±0.15	ND	ND	ND

C9-BA-DANA, C9-butyl-N-amide-DANA; DANA indicates 2,3-didehydro-2-deoxy-N-acetyl-neuraminic acid; ND, not determined; NEU1, neuraminidase 1; NEU2, neuraminidase 2; NEU3, neuraminidase 3; and NEU4, neuraminidase 4.

\*Full compound names, structures, and references provided in Figure S5.

†IC<sub>50</sub> and K<sub>i</sub> values were determined in our laboratory using the C1 carboxylate forms.<sup>12</sup>

### Pharmacological Inhibition of NEU1 and NEU3 Reduces Atherosclerosis in *Apoe*<sup>-/-</sup> and *Ldlr*<sup>-/-</sup> Mice

We hypothesized that if genetic ablation of NEU1 and NEU3 has preventive effect on atheroma formation, then pharmacological inhibition should provide similar outcome. To investigate this hypothesis, we used selective inhibitors of NEU1 and NEU3 enzymes with activity in the nanomolar range, developed in our laboratories<sup>14,51</sup> (Table and Figure S5). For comparison, we included in our study C9-BA-DANA, a NEU1 inhibitor with micromolar potency,<sup>52</sup> as well as the pan-sialidase inhibitor DANA (Table and Figure S5).

In the first experiment, 14-week-old *Apoe*<sup>-/-</sup> female mice received intraperitoneal injections of DANA (30 mg/kg BW) or C9-BA-DANA (30 mg/kg BW) dissolved in saline or saline alone. Inhibitors were administered for 2 weeks: once every 2 days for the first week, then every day for the second

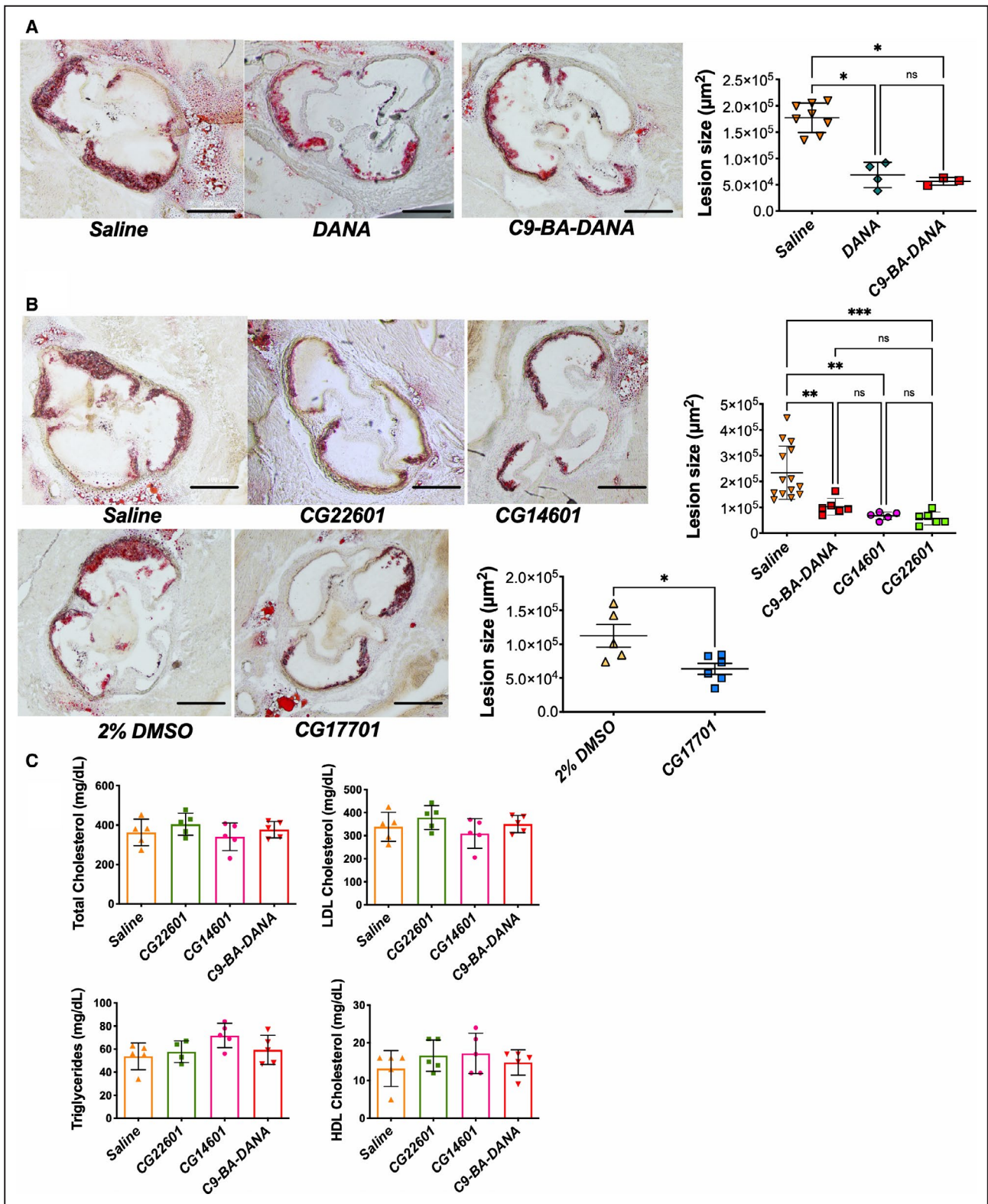
week. In a separate group of mice, the treatment was followed by histochemical analysis of neuraminidase activity in mouse kidney tissues, where the NEU1 isoform is responsible for >90% of total neuraminidase activity (Figure S6). This assay showed ≈70% to 80% reduction in tissue staining, consistent with almost complete inhibition of NEU1 activity (Figure S7). At 16 weeks, all mice were euthanized and atherosclerotic lesions were quantified in aortic root serial sections (Figure 6A). Both DANA and C9-BA-DANA treatments significantly reduced the size of atherosclerotic lesions in 16-week-old *Apoe*<sup>-/-</sup> mice. In both cases, the lesions were on average reduced to 25% to 30% of those in untreated *Apoe*<sup>-/-</sup> mice (Figure 6A). More important, inhibitor treatment had no observable effect on mouse weight or behavior.

In a second experiment, compounds with greater potency and selectivity for NEU1 or NEU3 were tested at lower dosages: CG17701 (an NEU3 and NEU4 inhibitor) at 1 mg/kg BW, CG14601 (an NEU1 inhibitor) at 10 mg/kg BW, and CG22601 (an

**Figure 6. Pharmacological inhibition of neuraminidase 1 (NEU1) and neuraminidase 3 (NEU3) reduces atherosclerosis in *Apoe*<sup>-/-</sup> mice.**

**A**, Reduced size of fatty streaks in the aortic root of 16-week-old *Apoe*<sup>-/-</sup> female mice treated for 2 weeks with pan-neuraminidase inhibitor 2,3-didehydro-2-deoxy-N-acetyl-neuraminic acid (DANA) and a NEU1 inhibitor, C9-butyl-N-amide-DANA (C9-BA-DANA). The 14-week-old *Apoe*<sup>-/-</sup> female mice fed normal diet were treated intraperitoneally with DANA (30 mg/kg; n=4) or with C9-BA-DANA (30 mg/kg; n=3) for 2 weeks, as described. Serial sections of aortic root (10 μm) were collected using a cryostat and stained with Red Oil O to visualize atherosclerotic lesions. Panels show representative images of aortic root sections. Bar=500 μm. Graph shows atherosclerotic lesion sizes in the aortic roots (μm<sup>2</sup>) measured by ImageJ software. Data show mean±SD. \*P<0.05 compared with control in Kruskal-Wallis test, followed by the Dunn multiple comparisons test. **B**, Reduced size of fatty streaks in the aortic root of 16-week-old *Apoe*<sup>-/-</sup> mice treated for 4 weeks with a NEU1-specific inhibitor, a NEU3-specific inhibitor, or a NEU3/neuraminidase 4-specific inhibitor. The 12-week-old *Apoe*<sup>-/-</sup> female mice fed normal diet received intraperitoneal injections of C9-BA-DANA (30 mg/kg; n=6), CG14601 (10 mg/kg body weight [BW]; n=5), and CG22601 (10 mg/kg BW; n=6) in saline or saline as a control (n=13). In a separate experiment, mice were treated with CG17701 (1 mg/kg BW; n=6) in saline with 2% dimethyl sulfoxide (DMSO) (v/v) or saline with 2% DMSO as a control (n=5) for 2 weeks. Then, the injections were performed every 24 hours for another 2 weeks, mice were euthanized at 16 weeks, and data were analyzed as described above. Panels show representative images of aortic root sections stained with Red Oil O. Bar=500 μm. Graphs show atherosclerotic lesion size in the aortic roots (μm<sup>2</sup>) measured by ImageJ software. Data show mean±SD. The lesion sizes in C9-BA-DANA-, CG14601-, and CG22601-treated mice were compared with the saline-treated control using Kruskal-Wallis test, followed by the Dunn multiple comparisons test. The lesion sizes in CG17701-treated mice were compared with the 2% DMSO-treated control using Mann-Whitney test. \*P<0.05, \*\*P<0.01, and \*\*\*P<0.001 compared with control. **C**, Lipid plasma composition of 16-week-old *Apoe*<sup>-/-</sup> mice treated for 4 weeks with NEU3-specific inhibitor and NEU1-specific inhibitors. Total cholesterol, triglyceride, high-density lipoprotein (HDL) cholesterol, and low-density lipoprotein (LDL) cholesterol levels were measured in mouse plasma samples after treatment with CG22601, CG14601, or C9-BA-DANA. Data represent mean±SD.





NEU3 inhibitor) at 10 mg/kg BW. Control mice were injected with saline or 2% DMSO (as the CG17701 control group). Because the previous study did not identify any obvious adverse effects of systematic

neuraminidase inhibition, treatments were extended to 1 month. Injections were started when mice were 12 weeks old, and were given once every 2 days for the first 2 weeks, then every day for the third and

the fourth weeks. Mice were then euthanized, and atherosclerotic lesions in serial sections of the aortic root were quantified, as above (Figure 6B).

Treatment with all 3 inhibitors significantly reduced the size of atherosclerotic lesions in *Apoe*<sup>-/-</sup> mice, with a 25% to 30% reduction on average compared with untreated *Apoe*<sup>-/-</sup> mice. Although the use of 2% DMSO alone reduced the lesion sizes (most likely because of previously described anti-inflammatory action of DMSO<sup>53</sup>), they were significantly larger than those in mice injected with CG17701 (Figure 6B). Again, pharmacological treatment did not affect mouse weight or behavior, or result in detectable pathological changes in tissues. Treatment with the inhibitors also did not affect the levels of total cholesterol, LDL cholesterol, HDL cholesterol, or triglycerides in the plasma of *Apoe*<sup>-/-</sup> mice (Figure 6C).

We further tested if NEU1 and NEU3 inhibitors also slow progression of atherosclerotic lesions in another commonly used mouse model of atherosclerosis, female hepatic LDLR knockout (*Ldlr*<sup>-/-</sup>) mice. These animals do not develop spontaneous lesions when fed the normal rodent diet, but show fatty streaks similar to those in *Apoe*<sup>-/-</sup> mice, when their food is supplemented with moderate amounts of cholesterol.<sup>54</sup> From the age of 8 weeks, *Ldlr*<sup>-/-</sup> mice were fed the diet containing 15% fat and 1.25% cholesterol, and, starting from 10 weeks, were treated with the most potent NEU1 and NEU3 inhibitors, CG14601 and CG22601, as described for *Apoe*<sup>-/-</sup> mice (the 4-week regimen). Then, mice were euthanized, and the areas of atherosclerotic lesions in the hearts were analyzed (Figure 7A). This analysis confirmed that, in both CG14601- and CG22601-treated mice, the development of lesions was significantly reduced compared with the control group. As in the case of *Apoe*<sup>-/-</sup> mice, treatment with the inhibitors did not affect the levels of total cholesterol, LDL cholesterol, HDL cholesterol, or triglycerides in the plasma of *Ldlr*<sup>-/-</sup> mice (Figure 7B).

## DISCUSSION

Previous observational data support a strong association between plasma LDL levels and augmented individual susceptibility to atherosclerosis and its complications, such as myocardial infarction and stroke. The current mainstay of therapeutic management of atherosclerosis is lowering LDL levels using inhibitors of hydroxymethyl glutaryl coenzyme A reductase, collectively known as statins, which diminish the likelihood of atherosclerotic events. However, statins only benefit ≈35% of patients with coronary artery disease.<sup>55</sup> Moreover, >20% of patients will have a recurrent event within 30 months of an acute coronary syndrome, despite receiving high-dose

statin treatment.<sup>56</sup> Together, the above evidence underlines the necessity of gaining further mechanistic insights into new targets for atherosclerosis therapeutic strategies.

Our current data demonstrate that desialylation of LDL by human neuraminidases constitutes a novel pathway contributing to atherosclerosis. It is now recognized that a major role in atherogenesis is played by biochemically modified LDLs, which have a longer circulation time because of a reduced affinity to LDLR<sup>11</sup> and can provoke a cascade of responses that lead to disease in a previously unaffected artery. We show herein that atherogenic LDL can be produced by removal of terminal Sia from the glycan chains of the major LDL surface glycoprotein, ApoB, by human neuraminidases in vitro. Desialylation of LDLs increases their affinity for the scavenger asialoglycoprotein receptor ASGR1, resulting in augmented uptake by intimal macrophages. We, however, do not see increased uptake of desLDL by either cultured HepG2 cells or hepatocytes in live mice. On the other hand, we observed a remarkable increase in the uptake of desLDL by liver macrophages (Kupffer cells). This result is somewhat unexpected considering that Ashwell-Morell receptor is highly expressed in the hepatocytes. We speculate that LDLR receptors on the surface of hepatocytes may play a predominant role in the uptake of LDL (whether native or desialylated). In contrast, for macrophages, the Asgr1-mediated uptake of desLDL makes drastic difference because these cells, in general, show limited uptake of native sialylated LDLs (Figure 1A). Besides, because our primary goal was to study LDL uptake by macrophages in the aortic sinus atheroma, in our studies, mice were euthanized 6 hours after LDL injection and, at this point, most Alexa-labeled LDL in hepatocytes could already be degraded.

The importance of Ashwell-Morell receptor pathway in atherosclerosis is strongly supported by the results of genome-wide association study that linked ASGR1 variant to a reduced risk of coronary artery disease in the population of Iceland.<sup>57</sup> The current results are also consistent with our previous data demonstrating abolished atheroma plaque size progression and decreased leukocyte infiltration in *Ldlr*<sup>-/-</sup> mice with 90% reduced NEU1 activity in cells of the hematopoietic lineage.<sup>25</sup> They also explain the mechanism underlying rapid endocytosis of LDL with low sialic acid content by human aortic intimal cells<sup>11</sup> and mouse peritoneal macrophages.<sup>58</sup>

While this article was under revision, White et al<sup>59</sup> reported reduced atherosclerosis in *Apoe*<sup>-/-</sup> mice carrying so-called *Neu1*<sup>hypo</sup> allele, a naturally occurring in SM/J mice Leu209Ile variant, presumably reducing neuraminidase activity in tissues to 50% to 60%. The authors explain the reduction of

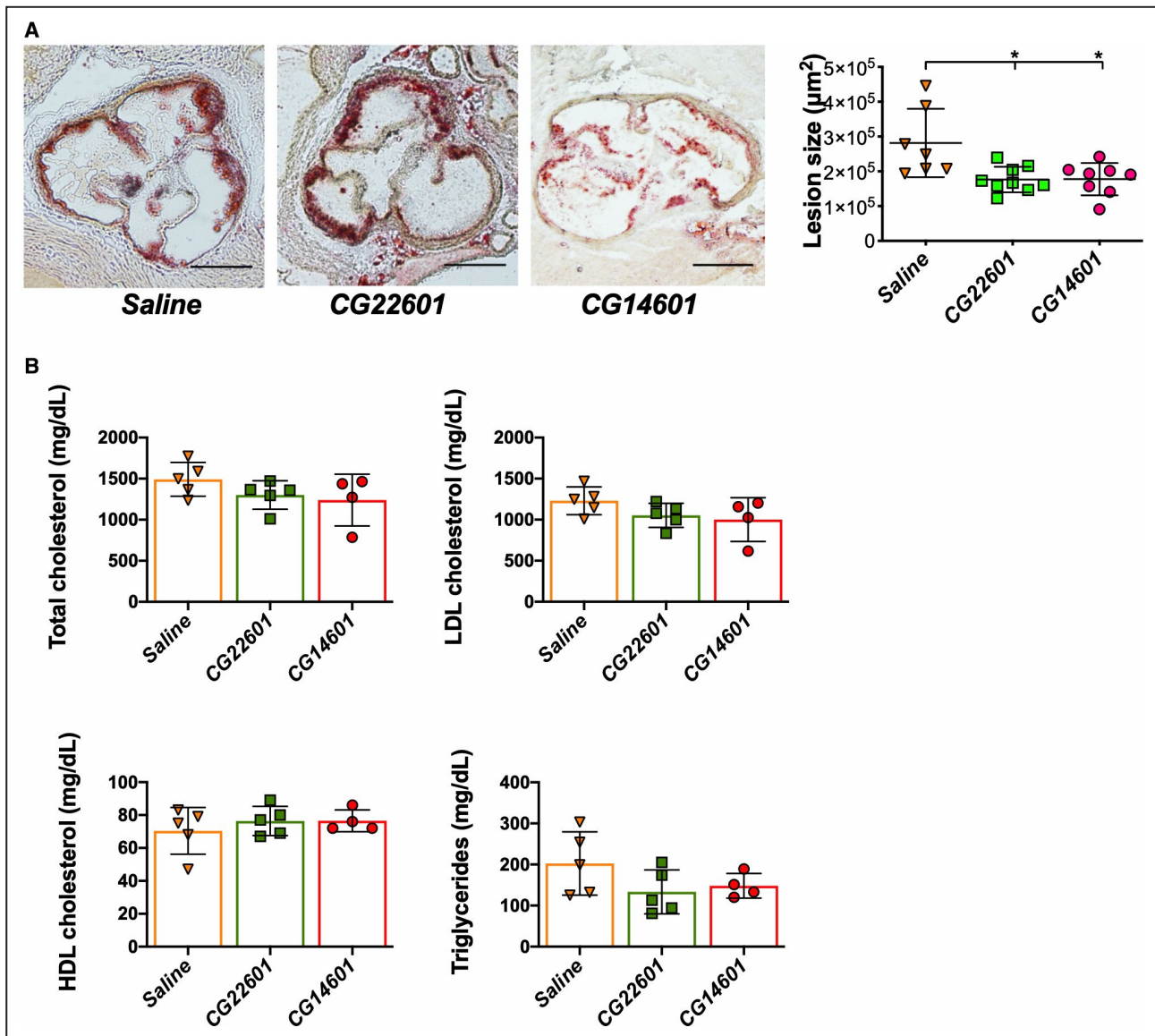


**Figure 7.** Pharmacological inhibition of neuraminidase 1 (NEU1) and neuraminidase 3 (NEU3) reduces atherosclerosis in *Ldlr*<sup>-/-</sup> mice.

**A**, Reduced size of fatty streaks in the aortic root of 14-week-old *Ldlr*<sup>-/-</sup> female mice treated with a NEU1-specific inhibitor and a NEU3-specific inhibitor. The 8-week-old *Ldlr*<sup>-/-</sup> female mice were fed a proatherogenic diet containing 15% fat and 1.25% cholesterol. Starting from 10 weeks, mice received intraperitoneal injections of sterile solutions of CG22601 (10 mg/kg body weight [BW]; n=9) and CG14601 (10 mg/kg BW; n=8) in saline every 48 hours for 2 weeks. The frequency of the injections was then increased to every 24 hours for another 2 weeks. Saline-treated mice were used as controls (n=7). Panels show representative images of aortic root sections stained with Red Oil O. Bar=500 µm. Graphs show atherosclerotic lesion size in the aortic roots (µm<sup>2</sup>) measured by ImageJ software. Data show mean±SD. \**P*<0.05 compared with control in Kruskal-Wallis multiple comparisons test. **B**, Lipid plasma composition of 14-week-old *Ldlr*<sup>-/-</sup> mice treated for 4 weeks with NEU1-specific inhibitor and NEU3-specific inhibitor. Total cholesterol, triglyceride, high-density lipoprotein (HDL) cholesterol, and low-density lipoprotein (LDL) cholesterol levels were measured in mouse plasma samples after treatment with CG22601 or CG14601. Data show individual and mean values (n=4 or 5)±SD.

atherosclerosis by decreased serum levels of very-low-density lipoprotein, LDL cholesterol, and circulating monocytes. In the present work, we do not detect changes in LDL cholesterol levels in *ApoE*<sup>-/-</sup> *CathA*<sup>S190A-Neo</sup> mice with 90% reduction of NEU1 activity, whereas we see increased LDL cholesterol in constitutive NEU1 knockout mice. Besides, in our

study, the reduction in size of the lesions in the NEU-deficient *ApoE*<sup>-/-</sup> mice does not directly correlate with the decrease in macrophage infiltration. Both lesion size and macrophage-positive area were reduced in NEU1-deficient mice. The *ApoE*<sup>-/-</sup> *Neu3*<sup>-/-</sup> mice did not show reduced macrophage infiltration compared with controls and, yet, had a reduced fatty streak

formation in the aortic root. This indicates that most likely a mechanism behind the reduced fatty streak formation is the reduction of macrophage uptake of desLDL and not the reduced macrophage content of the lesion. However, in *ApoE*<sup>-/-</sup> *CathA*<sup>S190A-Neo</sup> mice, atherosclerosis can be also slowed down by decreased monocyte/macrophage infiltration into the plaque. We also cannot completely exclude that a deficiency of cathepsin A activity affects atherogenesis in *CathA*<sup>S190A-Neo</sup> mice, although this seems unlikely considering that NEU1-specific inhibitors show similar antiatherosclerotic effect.

NEU1 and NEU3 can access LDL at the plasma membranes of circulating monocytes and tissue macrophages<sup>60-62</sup> as well as in plasma,<sup>42</sup> where both enzymes are present potentially as parts of extracellular vesicles.<sup>63</sup> Although both neuraminidases in the purified form have in vitro acidic pH optimum, they have been shown to be active at the membrane surface, most likely because of the presence of acidified microenvironment (reviewed by Pshezhetsky and Ashmarina<sup>64</sup>). Furthermore, the constant retroendocytosis of LDL via acidic endosomes<sup>65</sup> may also bring them in contact with neuraminidases inside the cell, resulting in progressive desialylation of ApoB oligosaccharide chains. The existence of this mechanism is supported by the large amount of desialylated oligosaccharides found in LDL from the blood of patients with coronary artery disease.<sup>7</sup>

Both NEU1 and NEU3 are induced in monocytes during their differentiation into macrophages and further during the activation of macrophages, where NEU1 is directly involved in induction of the inflammatory response.<sup>47,66-70</sup> Moreover, a recent study has directly demonstrated that NEU1 expression is drastically increased in macrophages in the intima layer, in calcified regions, and in the adventitia of the carotid artery plaques in human patients with atherosclerosis.<sup>66</sup> It is, therefore, tempting to speculate that the increase in desialylated LDL in circulation occurs in response to NEU1 induction associated with inflammation and atherosclerosis, resulting in a detrimental positive-feedback cycle: LDL desialylation→LDL uptake by macrophages→recruitment/activation of further macrophages→induction of NEU1/NEU3→LDL desialylation→LDL uptake by macrophages→foam cell formation→fatty streak formation. Our findings encourage further studies to test if low LDL sialylation and/or increased neuraminidase activity in leukocytes can serve as early biomarkers of atherosclerosis in a human population.

In addition to LDL uptake, neuraminidases may activate the earlier step of atherogenesis: the appearance of intercellular adhesion molecule 1 on the surface of endothelial cells, leading to an increase in binding and infiltration of leukocytes. Both NEU1 and NEU3 are expressed in human endothelial cells,

and NEU1 levels negatively correlate with their migration.<sup>71</sup> Moreover, removal of sialic acids from  $\beta$ 2-integrin (CD18 and CD11b) and of intercellular adhesion molecule 1 by polymorphonuclear leukocyte neuraminidase exposes activation epitopes, enhancing their interaction and resulting in tight adhesion between polymorphonuclear leukocytes and endothelial cells.<sup>72</sup> Atherosclerotic lesions are frequently found in areas of aortic endothelium with reduced sialic acid content, and removal of sialic acids from the intima of aorta by neuraminidases increases the adhesion of circulating platelets as well as the uptake of LDLs.<sup>73</sup> NEU3 can also modulate vascular smooth muscle cell response to inflammatory cytokines that may contribute to plaque instability in atherosclerosis.<sup>74</sup>

Our current data demonstrate that the genetic inactivation of both NEU1 and NEU3, but not of NEU4, reduces the rate of atherosclerosis in the *ApoE*<sup>-/-</sup> mice. Furthermore, we provide direct evidence that specific pharmacological inhibitors of these enzymes can have a therapeutic effect on the development of atherosclerotic lesions. These results make a compelling case for studying these inhibitors, or their analogs, as candidates for preventing or treating atherosclerosis. No diseases are associated with NEU3 genetic deficiency in humans, and *Neu3* knockout mice are viable, fertile, grow normally, and have normal life span. Although complete genetic inactivation of *NEU1* in humans blocks lysosomal catabolism of sialylated glycopeptides and oligosaccharides, and leads to severe neurological diseases sialidosis (Mendelian Inheritance in Man No. 256550) and galactosialidosis (Mendelian Inheritance in Man No. 256540), this does not preclude a possibility of a therapy based on partial or targeted NEU1 inhibition. The *CathA*<sup>S190A-Neo</sup> mouse model with  $\approx$ 10% residual activity of NEU1 in tissues used in this study is not clinically affected (unless challenged by a high-fat diet<sup>75</sup>), whereas a complete *Neu1* knockout mouse develops a systemic disease matching the human phenotype.<sup>46</sup> We speculate, therefore, that it would be possible to find a dose threshold for partial pharmacological inhibition of NEU1, providing a preventive or therapeutic effect for atherogenesis without affecting catabolic pathways for sialoglycoconjugates. Besides, it is possible that inhibition of specific NEU enzymes can affect the expression of other isoforms causing off-target effects, such as, observed in this study, changes in levels of plasma gangliosides in NEU1-deficient mice. Thus, definition of a therapeutic window may become a major challenge, and optimal dosing and duration will have to be carefully evaluated in future preclinical work. Besides, both safety and efficacy still need to be demonstrated in humans. However, overall, our study suggests that specific inhibitors of NEU1 and NEU3 or biological agents targeting these enzymes may become attractive candidates for preclinical evaluation.

## ARTICLE INFORMATION

Received August 25, 2020; accepted November 17, 2020.

### Affiliations

From the Departments of Pediatrics and Biochemistry, Sainte-Justine University Hospital Research Center, University of Montreal, Quebec, Canada (E.P.D., V.S., X.P., A.F., A.V.P.); Department of Chemistry, University of Alberta, Edmonton, Alberta, Canada (T.G., C.Z., R.C., C.W.C.); Departments of Medicine, Microbiology and Immunology, McGill University, Montreal, Quebec, Canada (B.D.S., D.C.S.); Department of Chemistry, Université du Québec à Montréal, Montreal, Quebec, Canada (T.C.S., R.R.); Institute of Human Morphology, Moscow, Russia (A.N.O.); Miyagi Cancer Center Research Institute, Natori, Miyagi, Japan (T.M.); and Institut National de la Santé et de la Recherche Médicale, UMR 1048, Institute of Metabolic and Cardiovascular Diseases, Toulouse, France (M.L.).

### Acknowledgments

The authors thank Carole Garofalo and Dr Emile Levy for the help with low-density lipoprotein purification, Anik Cloutier and Dr Anne-Monique Nuyt for the help with plasma lipid analysis, Ik-Hui Kho for the help with measuring neuraminidase activity in mouse tissues, and Dr Mila Ashmarina for critical reading of the manuscript.

Author contributions: conducted experiments and analyzed data: Drs Demina, Smutova, Pan, Fougerat, Guo, Zou, Chakraborty, Snarr, and Shiao; designed experiments and analyzed data: Drs Sheppard, Roy, Orekhov, Laffargue, Cairo, and Pshezhetsky; wrote and edited manuscript: Drs Demina, Smutova, Sheppard, Laffargue, Cairo, and Pshezhetsky; provided essential materials: Drs Miyagi, Roy, and Sheppard.

### Sources of Funding

This work was supported by the Canadian Glycomics Network (Project CD-2) and by Canadian Institutes of Health Research (Grant PJT-148863) to Drs Cairo and Pshezhetsky. Dr Roy thanks the Natural Sciences and Engineering Research Council of Canada and a Canada Research Chair for financial support. Dr Orekhov acknowledges financial support from the Russian Science Foundation (Grant 20-15-00264).

### Disclosures

A provisional patent application related to the inhibitors described in this study and their use in treatment of atherosclerosis has been filed by Drs Pshezhetsky, Cairo, and Guo. The remaining authors have no disclosures to report.

### Supplementary Material

Data S1

Tables S1–S4

Figures S1–S7

References 76–88

## REFERENCES

- Kalanur AA, Nyquist P, Ling G. The prevention and regression of atherosclerotic plaques: emerging treatments. *Vasc Health Risk Manag*. 2012;8:549–561.
- Weber C, Zernecke A, Libby P. The multifaceted contributions of leukocyte subsets to atherosclerosis: lessons from mouse models. *Nat Rev Immunol*. 2008;8:802–815.
- Bentzon JF, Otsuka F, Virmani R, Falk E. Mechanisms of plaque formation and rupture. *Circ Res*. 2014;114:1852–1866. DOI: 10.1161/CIRCRESAHA.114.302721.
- Packard RR, Libby P. Inflammation in atherosclerosis: from vascular biology to biomarker discovery and risk prediction. *Clin Chem*. 2008;54:24–38. DOI: 10.1373/clinchem.2007.097360.
- Millar JS. The sialylation of plasma lipoproteins. *Atherosclerosis*. 2001;154:1–13. DOI: 10.1016/S0021-9150(00)00697-3.
- Orekhov AN, Tertov VV, Mukhin DN. Desialylated low density lipoprotein—naturally occurring modified lipoprotein with atherogenic potency. *Atherosclerosis*. 1991;86:153–161. DOI: 10.1016/0021-9150(91)90211-K.
- Ruelland A, Gallou G, Legras B, Paillard F, Cloarec L. LDL sialic acid content in patients with coronary artery disease. *Clin Chim Acta*. 1993;221:127–133. DOI: 10.1016/0009-8981(93)90027-2.
- Tertov VV, Orekhov AN, Sobenin IA, Morrisett JD, Gotto AM Jr, Guevara JG Jr. Carbohydrate composition of protein and lipid components in sialic acid-rich and -poor low density lipoproteins from subjects with and without coronary artery disease. *J Lipid Res*. 1993;34:365–375.
- Lindberg G. Resialylation of sialic acid deficit vascular endothelium, circulating cells and macromolecules may counteract the development of atherosclerosis: a hypothesis. *Atherosclerosis*. 2007;192:243–245. DOI: 10.1016/j.atherosclerosis.2007.03.011.
- Bartlett AL, Grewal T, De Angelis E, Myers S, Stanley KK. Role of the macrophage galactose lectin in the uptake of desialylated LDL. *Atherosclerosis*. 2000;153:219–230. DOI: 10.1016/S0021-9150(00)00402-0.
- Tertov VV, Orekhov AN, Sobenin IA, Gabbasov ZA, Popov EG, Yaroslavov AA, Smirnov VN. Three types of naturally occurring modified lipoproteins induce intracellular lipid accumulation due to lipoprotein aggregation. *Circ Res*. 1992;71:218–228. DOI: 10.1161/01.RES.71.1.218.
- Guo T, Datwyler P, Demina E, Richards MR, Ge P, Zou C, Zheng R, Fougerat A, Pshezhetsky AV, Ernst B, et al. Selective inhibitors of human neuraminidase 3. *J Med Chem*. 2018;61:1990–2008. DOI: 10.1021/acs.jmedchem.7b01574.
- Fougerat A, Pan X, Smutova V, Heveker N, Cairo CW, Issat T, Larrivee B, Medin JA, Pshezhetsky AV. Neuraminidase 1 activates insulin receptor and reverses insulin resistance in obese mice. *Mol Metab*. 2018;12:76–88. DOI: 10.1016/j.molmet.2018.03.017.
- Zhang Y, Albohy A, Zou Y, Smutova V, Pshezhetsky AV, Cairo CW. Identification of selective inhibitors for human neuraminidase isoenzymes using C4, C7-modified 2-deoxy-2,3-didehydro-N-acetylneuraminic acid (DANA) analogues. *J Med Chem*. 2013;56:2948–2958.
- Levy E, Thibault L, Roy CC, Letarte J, Lambert M, Seidman EG. Mechanisms of hypercholesterolaemia in glycogen storage disease type I: defective metabolism of low density lipoprotein in cultured skin fibroblasts. *Eur J Clin Invest*. 1990;20:253–260. DOI: 10.1111/j.1365-2362.1990.tb01852.x.
- Smutova V, Albohy A, Pan X, Korchagina E, Miyagi T, Bovin N, Cairo CW, Pshezhetsky AV. Structural basis for substrate specificity of mammalian neuraminidases. *PLoS One*. 2014;9:e106320. DOI: 10.1371/journal.pone.0106320.
- Pitas RE, Innerarity TL, Weinstein JN, Mahley RW. Acetoacetylated lipoproteins used to distinguish fibroblasts from macrophages in vitro by fluorescence microscopy. *Arteriosclerosis*. 1981;1:177–185. DOI: 10.1161/01.ATV.1.3.177.
- Trouplin V, Boucherit N, Gorvel L, Conti F, Mottola G, Ghigo E. Bone marrow-derived macrophage production. *J Vis Exp*. 2013;81:e50966. DOI: 10.3791/50966.
- Zhang X, Goncalves R, Mosser DM. The isolation and characterization of murine macrophages. *Curr Protoc Immunol*. 2008;Chapter 14:Unit 14.1.
- Seyrantepe V, Hinek A, Peng J, Fedjaev M, Ernest S, Kadota Y, Canuel M, Itoh K, Morales CR, Lavoie J, et al. Enzymatic activity of lysosomal carboxypeptidase (cathepsin) A is required for proper elastic fiber formation and inactivation of endothelin-1. *Circulation*. 2008;117:1973–1981. DOI: 10.1161/CIRCULATIONAHA.107.733212.
- Seyrantepe V, Canuel M, Carpentier S, Landry K, Durand S, Liang F, Zeng J, Caqueret A, Gravel RA, Marchesini S, et al. Mice deficient in neu4 sialidase exhibit abnormal ganglioside catabolism and lysosomal storage. *Hum Mol Genet*. 2008;17:1556–1568.
- Yamaguchi K, Shiozaki K, Moriya S, Koseki K, Wada T, Tateno H, Sato I, Asano M, Iwakura Y, Miyagi T. Reduced susceptibility to colitis-associated colon carcinogenesis in mice lacking plasma membrane-associated sialidase. *PLoS One*. 2012;7:e41132.
- Chang CL, Seo T, Matsuzaki M, Worgall TS, Deckelbaum RJ. N-3 fatty acids reduce arterial LDL-cholesterol delivery and arterial lipoprotein lipase levels and lipase distribution. *Arterioscler Thromb Vasc Biol*. 2009;29:555–561.
- Pan X, De Aragao CBP, Velasco-Martin JP, Priestman DA, Wu HY, Takahashi K, Yamaguchi K, Sturiale L, Garozzo D, Platt FM, et al. Neuraminidases 3 and 4 regulate neuronal function by catabolizing brain gangliosides. *FASEB J*. 2017;31:3467–3483.
- Gayral S, Garnotel R, Castaing-Berthou A, Blaise S, Fougerat A, Berge E, Montheil A, Malet N, Wymann MP, Maurice P, et al. Elastin-derived peptides potentiate atherosclerosis through the immune Neu1-P13Kgamma pathway. *Cardiovasc Res*. 2014;102:118–127.

26. Allain CC, Poon LS, Chan CS, Richmond W, Fu PC. Enzymatic determination of total serum cholesterol. *Clin Chem*. 1974;20:470–475.
27. Roeschlau P, Bernt E, Gruber W. Enzymatic determination of total cholesterol in serum. *Z Klin Chem Klin Biochem*. 1974;12:226.
28. Albrecht S, Vainauskas S, Stockmann H, McManus C, Taron CH, Rudd PM. Comprehensive profiling of glycosphingolipid glycans using a novel broad specificity endoglycoceramidase in a high-throughput workflow. *Anal Chem*. 2016;88:4795–4802.
29. Sturgill ER, Aoki K, Lopez PH, Colacurcio D, Vajn K, Lorenzini I, Majic S, Yang WH, Heffer M, Tiemeyer M, et al. Biosynthesis of the major brain gangliosides gd1a and gt1b. *Glycobiology*. 2012;22:1289–1301.
30. Neville DC, Coquard V, Priestman DA, te Vruchte DJ, Sillence DJ, Dwek RA, Platt FM, Butters TD. Analysis of fluorescently labeled glycosphingolipid-derived oligosaccharides following ceramide glycanase digestion and anthranilic acid labeling. *Anal Biochem*. 2004;331:275–282.
31. Shibuya N, Goldstein IJ, Broekaert WF, Nsimba-Lubaki M, Peeters B, Peumans WJ. The elderberry (*Sambucus nigra* L.) bark lectin recognizes the Neu5Ac(alpha 2–6)Gal/GalNAc sequence. *J Biol Chem*. 1987;262:1596–1601.
32. Knibbs RN, Goldstein IJ, Ratcliffe RM, Shibuya N. Characterization of the carbohydrate binding specificity of the leukoagglutinating lectin from *Maackia amurensis*. comparison with other sialic acid-specific lectins. *J Biol Chem*. 1991;266:83–88.
33. Albohy A, Li MD, Zheng RB, Zou C, Cairo CW. Insight into substrate recognition and catalysis by the human neuraminidase 3 (NEU3) through molecular modeling and site-directed mutagenesis. *Glycobiology*. 2010;20:1127–1138.
34. Bartens W, Kramer-Guth A, Wanner C. Corticotropin increases the receptor-specific uptake of native low-density lipoprotein (LDL)—but not of oxidized LDL and native or oxidized lipoprotein(a) [Lp(a)]—in HEPG2 cells: no evidence for Lp(a) catabolism via the LDL-receptor. *Metabolism*. 1997;46:726–729.
35. Rhainds D, Falstra L, Tremblay C, Brissette L. Uptake and fate of class B scavenger receptor ligands in HepG2 cells. *Eur J Biochem*. 1999;261:227–235.
36. Sano H, Hsu DK, Apgar JR, Yu L, Sharma BB, Kuwabara I, Izui S, Liu FT. Critical role of galectin-3 in phagocytosis by macrophages. *J Clin Invest*. 2003;112:389–397.
37. Sorensen AL, Rumjantseva V, Nayeb-Hashemi S, Clausen H, Hartwig JH, Wandall HH, Hoffmeister KM. Role of sialic acid for platelet life span: exposure of beta-galactose results in the rapid clearance of platelets from the circulation by asialoglycoprotein receptor-expressing liver macrophages and hepatocytes. *Blood*. 2009;114:1645–1654.
38. Windler E, Greeve J, Levkau B, Kolb-Bachofen V, Daerr W, Greten H. The human asialoglycoprotein receptor is a possible binding site for low-density lipoproteins and chylomicron remnants. *Biochem J*. 1991;276(pt 1):79–87.
39. Harris RL, van den Berg CW, Bowen DJ. ASGR1 and ASGR2, the genes that encode the asialoglycoprotein receptor (Ashwell receptor), are expressed in peripheral blood monocytes and show interindividual differences in transcript profile. *Mol Biol Int*. 2012;2012:283974.
40. Yang EH, Rode J, Howlader MA, Eckermann M, Santos JT, Hernandez Armada D, Zheng R, Zou C, Cairo CW. Galectin-3 alters the lateral mobility and clustering of beta1-integrin receptors. *PLoS One*. 2017;12:e0184378.
41. Hsu DK, Yang RY, Pan Z, Yu L, Salomon DR, Fung-Leung WP, Liu FT. Targeted disruption of the galectin-3 gene results in attenuated peritoneal inflammatory responses. *Am J Pathol*. 2000;156:1073–1083. DOI: 10.1016/S0002-9440(10)64975-9.
42. Yang WH, Aziz PV, Heithoff DM, Mahan MJ, Smith JW, Marth JD. An intrinsic mechanism of secreted protein aging and turnover. *Proc Natl Acad Sci USA*. 2015;112:13657–13662. DOI: 10.1073/pnas.1515464112.
43. Piedrahita JA, Zhang SH, Hagan JR, Oliver PM, Maeda N. Generation of mice carrying a mutant apolipoprotein E gene inactivated by gene targeting in embryonic stem cells. *Proc Natl Acad Sci USA*. 1992;89:4471–4475. DOI: 10.1073/pnas.89.10.4471.
44. Jawien J, Nastalek P, Korbut R. Mouse models of experimental atherosclerosis. *J Physiol Pharmacol*. 2004;55:503–517.
45. Meir KS, Leitersdorf E. Atherosclerosis in the apolipoprotein-E-deficient mouse: a decade of progress. *Arterioscler Thromb Vasc Biol*. 2004;24:1006–1014. DOI: 10.1161/01.ATV.0000128849.12617.f4.
46. de Geest N, Bonten E, Mann L, de Sousa-Hitzler J, Hahn C, d’Azzo A. Systemic and neurologic abnormalities distinguish the lysosomal disorders sialidosis and galactosialidosis in mice. *Hum Mol Genet*. 2002;11:1455–1464. DOI: 10.1093/hmg/11.12.1455.
47. Amith SR, Jayanth P, Franchuk S, Siddiqui S, Seyrantepe V, Gee K, Basta S, Beyaert R, Pshezhetsky AV, Szewczuk MR. Dependence of pathogen molecule-induced toll-like receptor activation and cell function on Neu1 sialidase. *Glycoconj J*. 2009;26:1197–1212. DOI: 10.1007/s10719-009-9239-8.
48. Amith SR, Jayanth P, Franchuk S, Finlay T, Seyrantepe V, Beyaert R, Pshezhetsky AV, Szewczuk MR. Neu1 desialylation of sialyl alpha-2,3-linked beta-galactosyl residues of Toll-like receptor 4 is essential for receptor activation and cellular signaling. *Cell Signal*. 2010;22:314–324.
49. Senn HJ, Orth M, Fitzke E, Wieland H, Gerok W. Gangliosides in normal human serum: concentration, pattern and transport by lipoproteins. *Eur J Biochem*. 1989;181:657–662. DOI: 10.1111/j.1432-1033.1989.tb14773.x.
50. Cotterchio M, Seyfried TN. Serum gangliosides in mice with metastatic and non-metastatic brain tumors. *J Lipid Res*. 1994;35:10–14.
51. Albohy A, Zhang Y, Smutova V, Pshezhetsky AV, Cairo CW. Identification of selective nanomolar inhibitors of the human neuraminidase, NEU4. *AACS Med Chem Lett*. 2013;4:532–537.
52. Magesh S, Moriya S, Suzuki T, Miyagi T, Ishida H, Kiso M. Design, synthesis, and biological evaluation of human sialidase inhibitors, part 1: selective inhibitors of lysosomal sialidase (NEU1). *Bioorg Med Chem Lett*. 2008;18:532–537. DOI: 10.1016/j.bmcl.2007.11.084.
53. Fani K, Debons AF, Jimenez FA, Hoover EL. Cholesterol-induced atherosclerosis in the rabbit: effect of dimethyl sulfoxide on existing lesions. *J Pharmacol Exp Ther*. 1988;244:1145–1149.
54. Ishibashi S, Brown MS, Goldstein JL, Gerard RD, Hammer RE, Herz J. Hypercholesterolemia in low density lipoprotein receptor knockout mice and its reversal by adenovirus-mediated gene delivery. *J Clin Invest*. 1993;92:883–893. DOI: 10.1172/JCI116663.
55. Arsenault BJ, Kritkou EA, Tardif JC. Regression of atherosclerosis. *Curr Cardiol Rep*. 2012;14:443–449. DOI: 10.1007/s11886-012-0285-7.
56. Cannon CP, Braunwald E, McCabe CH, Rader DJ, Rouleau JL, Belder R, Joyal SV, Hill KA, Pfeffer MA, Skene AM. Intensive versus moderate lipid lowering with statins after acute coronary syndromes. *N Engl J Med*. 2004;350:1495–1504. DOI: 10.1056/NEJMoa040583.
57. Nioi P, Sigurdsson A, Thorleifsson G, Helgason H, Jonasdottir AB, Norddahl GL, Helgadottir A, Magnusdottir A, Jonasdottir A, Gretarsdottir S, et al. Variant ASGR1 associated with a reduced risk of coronary artery disease. *N Engl J Med*. 2016;374:2131–2141.
58. Grewal T, Bartlett A, Burgess JW, Packer NH, Stanley KK. Desialylated LDL uptake in human and mouse macrophages can be mediated by a lectin receptor. *Atherosclerosis*. 1996;121:151–163. DOI: 10.1016/0021-9150(95)05715-3.
59. White EJ, Gyulay G, Lhoták Š, Szewczyk MM, Chong T, Fuller MT, Dadoo O, Fox-Robichaud AE, Austin RC, Trigatti BL, et al. Sialidase down-regulation reduces non-HDL cholesterol, inhibits leukocyte transmigration, and attenuates atherosclerosis in ApoE knockout mice. *J Biol Chem*. 2018;293:14689–14706. DOI: 10.1074/jbc.RA118.004589.
60. Wang Y, Yamaguchi K, Wada T, Hata K, Zhao X, Fujimoto T, Miyagi T. A close association of the ganglioside-specific sialidase Neu3 with caveolin in membrane microdomains. *J Biol Chem*. 2002;277:26252–26259. DOI: 10.1074/jbc.M110515200.
61. Zanchetti G, Colombi P, Manzoni M, Anastasia L, Caimi L, Borsani G, Venerando B, Tettamanti G, Preti A, Monti E, et al. Sialidase NEU3 is a peripheral membrane protein localized on the cell surface and in endosomal structures. *Biochem J*. 2007;408:211–219. DOI: 10.1042/BJ20070503.
62. Lukrong KE, Seyrantepe V, Landry K, Trudel S, Ahmad A, Gahl WA, LeFrancis S, Morales CR, Pshezhetsky AV. Intracellular distribution of lysosomal sialidase is controlled by the internalization signal in its cytoplasmic tail. *J Biol Chem*. 2001;276:46172–46181. DOI: 10.1074/jbc.M104547200.
63. Paolini L, Orizio F, Busatto S, Radeghieri A, Bresciani R, Bergese P, Monti E. Exosomes secreted by HeLa cells shuttle on their surface the plasma membrane-associated sialidase NEU3. *Biochemistry*. 2017;56:6401–6408. DOI: 10.1021/acs.biochem.7b00665.
64. Pshezhetsky AV, Ashmarina M. Keeping it trim: roles of neuraminidases in CNS function. *Glycoconj J*. 2018;35:375–386. DOI: 10.1007/s10719-018-9837-4.
65. Snyder ML, Polacek D, Scanu AM, Fless GM. Comparative binding and degradation of lipoprotein(a) and low density lipoprotein by human monocyte-derived macrophages. *J Biol Chem*. 1992;267:339–346.

66. Sieve I, Ricke-Hoch M, Kasten M, Battmer K, Stapel B, Falk CS, Leisegang MS, Haverich A, Scherr M, Hilfiker-Kleiner D. A positive feedback loop between IL-1 $\beta$ , LPS and NEU1 may promote atherosclerosis by enhancing a pro-inflammatory state in monocytes and macrophages. *Vascul Pharmacol*. 2018;103–105:16–28.
67. Stamatou NM, Liang F, Nan X, Landry K, Cross AS, Wang LX, Pshezhetsky AV. Differential expression of endogenous sialidases of human monocytes during cellular differentiation into macrophages. *FEBS J*. 2005;272:2545–2556. DOI: 10.1111/j.1742-4658.2005.04679.x.
68. Seyrantepe V, Iannello A, Liang F, Kanshin E, Jayanth P, Samarani S, Szwedczuk MR, Ahmad A, Pshezhetsky AV. Regulation of phagocytosis in macrophages by neuraminidase 1. *J Biol Chem*. 2010;285:206–215. DOI: 10.1074/jbc.M109.055475.
69. Liang F, Seyrantepe V, Landry K, Ahmad R, Ahmad A, Stamatou NM, Pshezhetsky AV. Monocyte differentiation up-regulates the expression of the lysosomal sialidase, Neu1, and triggers its targeting to the plasma membrane via major histocompatibility complex class II-positive compartments. *J Biol Chem*. 2006;281:27526–27538. DOI: 10.1074/jbc.M605633200.
70. Chen GY, Brown NK, Wu W, Khedri Z, Yu H, Chen X, van de Vlekkert D, D'Azzo A, Zheng P, Liu Y. Broad and direct interaction between TLR and Siglec families of pattern recognition receptors and its regulation by Neu1. *Elife*. 2014;3:e04066.
71. Cross AS, Hyun SW, Miranda-Ribera A, Feng C, Liu A, Nguyen C, Zhang L, Luzina IG, Atamas SP, Twaddell WS, et al. NEU1 and NEU3 sialidase activity expressed in human lung microvascular endothelia: NEU1 restrains endothelial cell migration, whereas NEU3 does not. *J Biol Chem*. 2012;287:15966–15980.
72. Feng C, Zhang L, Almulki L, Faez S, Whitford M, Hafezi-Moghadam A, Cross AS. Endogenous PMN sialidase activity exposes activation epitope on CD11b/CD18 which enhances its binding interaction with ICAM-1. *J Leukoc Biol*. 2011;90:313–321.
73. Gorog P, Born GV. Uneven distribution of sialic acids on the luminal surface of aortic endothelium. *Br J Exp Pathol*. 1983;64:418–424.
74. Moon SK, Cho SH, Kim KW, Jeon JH, Ko JH, Kim BY, Kim CH. Overexpression of membrane sialic acid-specific sialidase Neu3 inhibits matrix metalloproteinase-9 expression in vascular smooth muscle cells. *Biochem Biophys Res Commun*. 2007;356:542–547.
75. Dridi L, Seyrantepe V, Fougerat A, Pan X, Bonneil E, Thibault P, Moreau A, Mitchell GA, Heveker N, Cairo CW, et al. Positive regulation of insulin signaling by neuraminidase 1. *Diabetes*. 2013;62:2338–2346.
76. Harazono A, Kawasaki N, Kawanishi T, Hayakawa T. Site-specific glycosylation analysis of human apolipoprotein B100 using LC/ESI MS/MS. *Glycobiology*. 2005;15:447–462.
77. Richards MR, Guo T, Hunter CD, Cairo CW. Molecular dynamics simulations of viral neuraminidase inhibitors with the human neuraminidase enzymes: insights into isoenzyme selectivity. *Bioorg Med Chem*. 2018;26:5349–5358.
78. Guo T, Héon-Roberts R, Zou C, Zheng R, Pshezhetsky AV, Cairo CW. Selective inhibitors of human neuraminidase 1 (NEU1). *J Med Chem*. 2018;61:11261–11279.
79. Cao S, Meunier SJ, Andersson FO, Letellier M, Roy R. Mild stereoselective syntheses of thioglycosides under PTC conditions and their use as active and latent glycosyl donors. *Tetrahedron Asymmetry*. 1994;5:2303–2312.
80. Carrière D, Meunier S, Tropper F, Cao S, Roy R. Phase transfer catalysis toward the synthesis of O-, S-, Se- and C-glycosides. *J Mol Catal A Chem*. 2000;154:9–22.
81. Roy R. Phase transfer catalysis in carbohydrate chemistry. In: Sasson Y, Neumann R, eds. *Handbook of Phase Transfer Catalysis*. London: Springer; 1997:244–275.
82. Roy R, Tropper F, Cao S, Kim J. Anomeric group transformations under phase-transfer catalysis. In: Halpern ME, ed. *Phase-Transfer Catalysis*. Washington, DC: ACS Publications; 1997:163–180.
83. Tropper FD, Andersson FO, Braun S, Roy R. Phase transfer catalysis as a general and stereoselective entry into glycosyl azides from glycosyl halides. *Synthesis*. 1992;1992:618–620.
84. Tropper FD, Andersson FO, Grand-Maitre C, Roy R. Stereospecific synthesis of 1, 2-trans-1-phenylthio- $\beta$ -D-disaccharides under phase transfer catalysis. *Synthesis*. 1991;1991:734–736.
85. Shiao TC, Giguère D, Galanos N, Roy R. Efficient synthesis of hepta-O-acetyl- $\beta$ -lactosyl azide via phase transfer catalysis. In: van der Marel G, Codee J, eds. *Carbohydrate Chemistry*. Boca Raton, FL: CRC Press; 2014:296–301.
86. Šardžik R, Noble GT, Weissenborn MJ, Martin A, Webb SJ, Flitsch SL. Preparation of aminoethyl glycosides for glycoconjugation. *Beilstein J Org Chem*. 2010;6:699–703.
87. Johnsson R, Meijer A, Ellervik U. Mild and efficient direct aromatic iodination. *Tetrahedron*. 2005;61:11657–11663.
88. Rodrigue J, Ganne G, Blanchard B, Saucier C, Giguère D, Shiao TC, Varrot A, Imberty A, Roy R. Aromatic thioglycoside inhibitors against the virulence factor LecA from *Pseudomonas aeruginosa*. *Org Biomol Chem*. 2013;11:6906–6918.

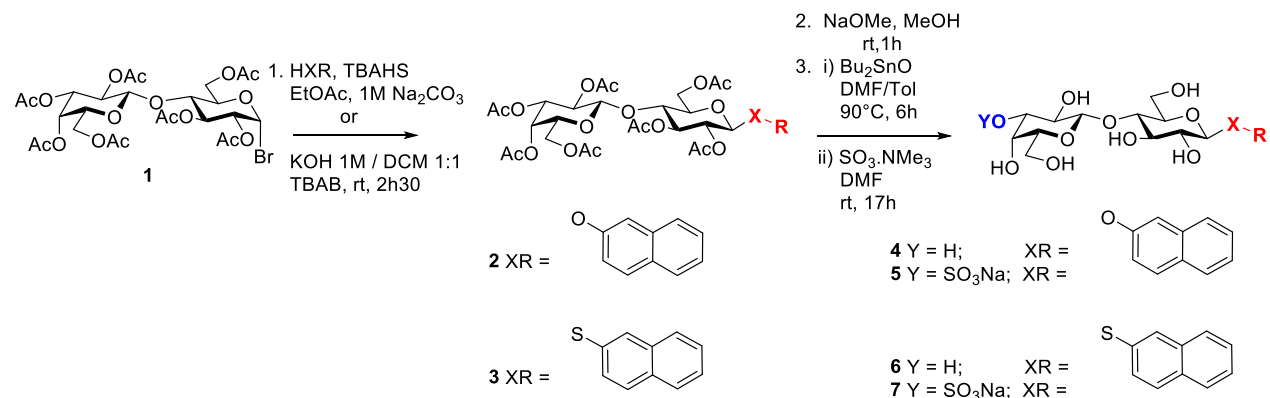
# **SUPPLEMENTAL MATERIAL**



## Data S1.

### Supplemental Methods

#### Synthesis of 3'-*O*-sulfated lactoside galectin inhibitors (Lot 20160705)



**Scheme 1.** Synthetic steps leading to lactoside analogs and their 3'-*O*-sulfated derivatives.

#### General synthetic methods

All reactions in organic medium were performed in standard oven dried glassware under an inert atmosphere of nitrogen using freshly distilled solvents. Solvents and reagents were deoxygenated, when necessary by purging with nitrogen. All reagents were used as supplied without prior purification unless otherwise stated, and obtained from Sigma-Aldrich Chemical Co. Ltd. Reactions were monitored by analytical thin-layer chromatography (TLC) using silica gel 60 F254 precoated plates (E. Merck) and compounds were visualized with a 254 nm UV lamp, a mixture of iodine/silica gel and/or mixture of ceric ammonium molybdate solution (100 mL H<sub>2</sub>SO<sub>4</sub>, 900 mL H<sub>2</sub>O, 25 g (NH<sub>4</sub>)<sub>6</sub>Mo<sub>7</sub>O<sub>24</sub>H<sub>2</sub>O, 10 g Ce(SO<sub>4</sub>)<sub>2</sub>) and subsequent spots development by gentle warming with a heat-gun. Purifications were performed by silica gel flash column chromatography using Silicycle (60 Å, 40-63 μm) with the indicated eluent. NMR spectroscopy was used to record <sup>1</sup>H NMR and <sup>13</sup>C NMR spectra at 300 and at 75 MHz, respectively, on Bruker 300 MHz spectrometers. Proton and carbon chemical shifts (δ) are reported in ppm relative to the chemical shift of residual CHCl<sub>3</sub>, which was set at 7.27 ppm (<sup>1</sup>H) and 77.00 ppm (<sup>13</sup>C). Coupling constants (*J*) are reported in Hertz (Hz), and the following abbreviations are used for peak multiplicities: singlet (s), doublet (d), doublet of doublets (dd), doublet of doublet with equal coupling constants (t<sub>ap</sub>), triplet (t), multiplet (m). Analysis and assignments were made using COSY (COrrrelated Spectroscopy) and HSQC (Heteronuclear Single Quantum Coherence) experiments. High-resolution mass spectrometry (HRMS) data were measured with a LC-MS-TOF (Liquid Chromatography-Mass Spectrometry-Time Of Flight; Agilent Technologies) in positive and/or negative electrospray mode(s) at the analytical platform of UQAM.

**General synthetic procedure A: phase-Transfer Catalysis (PTC) reaction.** PTC reactions were performed following the previously established protocols<sup>80-85</sup> or under the slightly modified procedure as follows: to a solution of peracetylated lactosyl bromide **1** (Scheme 1)<sup>86</sup> (1 equiv.) in dichloromethane (6 mL) was added the corresponding aromatic alcohol (1 equiv.),

tetrabutylammonium bromide (TBAB, 0.5 equiv.) and KOH (1M, 6 equiv.). The mixture was stirred at room temperature for two h 30 min and then washed successively with water and brine. The organic layer was dried over Na<sub>2</sub>SO<sub>4</sub> and concentrated under reduced pressure. Purification by silica gel column chromatography (Hex/AcOEt: 7/3) afforded the corresponding compounds **2** and **3** as yellow oil (yield 70-81%).

**General synthetic procedure B: Zemplén transesterification reaction:** To a solution of lactoside **2** and **3** in dry methanol was added a solution of sodium methoxide (1 M in MeOH, 0.1 equiv.). After stirring at room temperature for 1 h, the reaction was completed and then neutralized by addition of ion-exchange resin (Amberlite IR 120 H<sup>+</sup>). The solution was filtered and evaporated *in vacuo* to afford the de-*O*-acetylated lactosides **4** and **6** as white powder (yield 95%-quant.)

**General synthetic procedure C: preparation of 3'-*O*-sulfated lactosides:** A mixture of deacetylated lactoside **4** and **6** (1 equiv.) and dibutyltin oxide (1.15 equiv.) in DMF/toluene (6 mL/3 mL) were stirred at 90°C for 6 h. The solution was then concentrated and Me<sub>3</sub>N·SO<sub>3</sub> (1.3 equiv.) and dry DMF (6 mL) were added. After stirring at room temperature for 17 h, the reaction was quenched with water and evaporated under vacuum. The residue was purified through a column of DOWEX Marathon C (Na<sup>+</sup>) and eluted with H<sub>2</sub>O to afford the pure 3'-*O*-sulfated lactosides **5** and **7** as white powder after lyophilization (yield 80-84%).

#### **2,3,6,2',3',4',6'-Hepta-*O*-acetyl-β-d-lactopyranosyl bromide (1)**

To a solution of per-*O*-acetylated lactose<sup>86</sup> (14.2 g, 21 mmol) in anhydrous CH<sub>2</sub>Cl<sub>2</sub> (63 mL) was added hydrobromic acid (33% in AcOH, 47.9 mL). The reaction mixture was stirred at room temperature for 1 h, then neutralized with saturated aqueous NaHCO<sub>3</sub> and washed with brine. The organic layer was dried over Na<sub>2</sub>SO<sub>4</sub> and concentrated under reduced pressure to afford lactosyl bromide **1** (13.6 g, 93%) as a white solid. Its spectroscopic data agreed well with those of the literature.<sup>87</sup>

#### **2-Naphthyl 2,3,6,2',3',4',6'-hepta-*O*-acetyl-β-d-lactopyranoside (2)**

Following the general procedure A. Compound **2** was obtained as a yellow oil, yield: 556 mg (73%), *R<sub>f</sub>* 0.5 (Hex/EtOAc: 1/1). <sup>1</sup>H NMR (300 MHz, CDCl<sub>3</sub>): δ 7.74-7.64 (m, 3H, Ar), 7.40-7.32 (m, 2H, Ar), 7.26 (d, 1H, Ar), 7.12-7.08 (dd, 1H, Ar), 5.37-5.36 (m, 1H, H-4'), 5.33-5.27 (m, 1H, H-3), 5.27-5.18 (m, 2H), 5.0-5.96 (dd, 1H), 4.55-4.52 (m, 2H), 4.20-4.07 (m, 3H), 3.96-3.85 (m, 3H), 2.17-1.98 (21H, 7OAc). Spectroscopic data agrees with those of the literature.<sup>88</sup>

#### **2-Naphthyl 2,3,6,2',3',4',6'-hepta-*O*-acetyl-1-thio-β-d-lactopyranoside (3)**

Following the general procedure A. Compound **3** was obtained as a yellow oil, yield: 650 mg (83%), *R<sub>f</sub>* 0.52 (Hex/EtOAc: 1/1). <sup>1</sup>H NMR (300 MHz, CDCl<sub>3</sub>): δ 7.95 (d, 1H, *J* = 1.2 Hz, Ar), 7.81-7.73 (m, 3H, Ar), 7.53-7.45 (m, 3H, Ar), 5.31-5.28 (m, 1H, H-4'), 5.21 (t, 1H, H-3), 5.10-5.04 (dd, 1H, H-2'), 4.95-4.93 (m, 1H, H-3'), 4.90 (t, 1H, H-2), 4.75 (d, 1H, *J* = 10.0 Hz, H-1), 4.54-4.49 (m, 1H, H-6a), 4.47 (d, 1H, *J* = 7.8 Hz, H-1'), 4.12-4.10 (m, 1H, H-6b), 4.08-4.04 (m, 2H, H-6'ab), 3.85 (t, 1H, *J* = 6.7 Hz, H-5'), 3.72 (t, 1H, H-4), 3.69-3.65 (m, 1H, H-5), 2.13-1.93 (21H, 7OAc). Spectroscopic data agrees with those previously reported.<sup>89</sup>

#### **2-Naphthyl β-d-lactopyranoside (4)**

Following the general procedure B. Compound **4** was obtained as a white powder, yield: 209 mg (95%), *R<sub>f</sub>* 0.55 (CH<sub>2</sub>Cl<sub>2</sub>/MeOH: 7/3). <sup>1</sup>H NMR (300 MHz, MeOD): δ 7.82-7.78 (m, 3H, Ar), 7.50-7.29 (m, 4H, Ar), 5.14 (d, 1H, *J* = 7.62 Hz, H-1), 4.45 (d, 1H, *J* = 7.5 Hz, H-1'), 4.02-3.90 (m, 2H, *J* = 10.86 Hz, H-6'), 3.86 (m, 1H, H-4'), 3.84-3.75 (m, 2H, *J* = 11.4 Hz, H-6), 3.73-3.71 (m, 3H, H-3,4,5'), 3.66 (m, 1H, *J* = 7.62 Hz, H-2), 3.64 (m, 1H, H-5), 3.60 (m, 1H, *J* = 7.5 Hz, H-2'), 3.55-3.50 (m, 1H, H-3').

<sup>13</sup>C NMR (75 MHz, MeOD): δ 155.3 (Cq Ar), 134.5 (Cq Ar), 129.9 (Cq Ar), 128.9, 127.2, 126.7, 125.9, 123.8, 118.5, 110.6, 103.6 (C-1'), 100.7 (C-1), 78.8 (C-5'), 75.7 (C-5), 75.3 and 74.9 (C-3,4), 73.4 (C-3'), 73.2 (C-2), 71.1 (C-2'), 68.9 (C-4'), 61.1 (C-6), 60.3 (C-6'). ESI-HRMS: *m/z* calcd for C<sub>22</sub>H<sub>28</sub>O<sub>11</sub>, 468.1632; found 468.1608.

#### **2-Naphthyl 3'-O-sulfo-β-d-lactopyranoside, sodium salt (5)**

Following the general procedure C. Compound **5** was obtained as a white powder, yield: 136 mg (80%), *R<sub>f</sub>* 0.48 (CH<sub>2</sub>Cl<sub>2</sub>/MeOH: 7/3). <sup>1</sup>H NMR (300 MHz, D<sub>2</sub>O): δ 7.85-7.77 (m, 3H, Ar), 7.5-7.42 (m, 3H, Ar), 7.27 (d, 1H, *J* = 9 Hz, Ar), 5.15 (d, 1H, *J* = 7.41 Hz, H-1), 4.51 (d, 1H, *J* = 7.7 Hz, H-1'), 4.28 (dd, 1H, *J* = 3.3, 9.7 Hz, H-3'), 4.22 (m, 1H, *J* = 3.3 Hz, H-4'), 3.95 (d, 1H, *J* = 11.58 Hz, H-6a), 3.75 (d, 1H, *J* = 11.58 Hz, H-6b), 3.71-3.66 (m, 6H, H-3,4,5,5',6'ab), 3.64 (dd, 1H, *J* = 7.7, 9.7 Hz, H-2'), 3.59 (m, 1H, H-2). <sup>13</sup>C NMR (75 MHz, D<sub>2</sub>O): δ 154.3 (Cq Ar), 133.8 (Cq Ar), 129.9, 129.7 (Cq Ar), 127.7, 127.1, 126.9, 124.9, 118.5, 110.7, 102.5 (C-1'), 99.9 (C-1), 80.0 (C-3'), 78.0 (C-5), 74.9 (C-3,5'), 74.1 (C-4), 72.6 (C-2), 69.1 (C-2'), 66.8 (C-4'), 60.8 (C-6'), 60.0 (C-6). ESI-HRMS: *m/z* calcd for C<sub>22</sub>H<sub>28</sub>O<sub>14</sub>S, 548.1216; found 547.1144 [M-H].

#### **2-Naphthyl 1-thio-β-d-lactopyranoside (6)**

Following the general procedure B. Compound **6** was obtained as a white powder, yield: 401 mg (quant.), *R<sub>f</sub>* 0.57 (CH<sub>2</sub>Cl<sub>2</sub>/MeOH: 7/3). <sup>1</sup>H NMR (300 MHz, MeOD): δ 8.10 (s, 1H, Ar), 7.85-7.80 (m, 3H, Ar), 7.68-7.65 (m, 1H, Ar), 7.53-7.48 (m, 2H, Ar), 4.76 (d, 1H, *J* = 9.0 Hz, H-1), 4.39 (d, 1H, *J* = 7.38 Hz, H-1'), 3.99-3.85 (m, 2H, H-6'), 3.82 (m, 1H, H-4'), 3.79-3.67 (m, 2H, H-6), 3.61-3.59 (m, 3H, H-3,4,5), 3.57 (m, 1H, H-2'), 3.53 (m, 1H, H-5'), 3.51-3.47 (m, 1H, H-3'), 3.37-3.36 (m, 1H, H-2). <sup>13</sup>C NMR (75 MHz, MeOD): δ 132.6 (Cq Ar), 130.9 (Cq Ar), 130.3, 129.1 (Cq Ar), 129.0, 127.8, 127.2, 127.1, 126.1, 125.8, 103.5 (C-1'), 87.6 (C-1), 79.2 (C-5'), 78.7 (C-5), 76.6 and 75.7 (C-3,4), 73.4 (C-3'), 72.0 (C-2), 71.1 (C-2'), 68.9 (C-4'), 61.1 (C-6), 60.6 (C-6'). ESI-HRMS: *m/z* calcd for C<sub>22</sub>H<sub>28</sub>O<sub>10</sub>S, 484.1403; found 484.1446.

#### **2-Naphthyl 3'-O-sulfo-1-thio-β-d-lactopyranoside, sodium salt (7)**

Following the general procedure C. Compound **7** was obtained as a white powder, yield: 119 mg (84%), *R<sub>f</sub>* 0.5 (CH<sub>2</sub>Cl<sub>2</sub>/MeOH: 7/3). <sup>1</sup>H NMR (300 MHz, D<sub>2</sub>O): δ 7.92 (s, 1H, Ar), 7.79-7.72 (m, 3H, Ar), 7.5-7.4 (m, 3H, Ar), 4.74 (d, 1H, *J* = 8.82 Hz, H-1), 4.42 (d, 1H, *J* = 7.83 Hz, H-1'), 4.23 (dd, 1H, *J* = 3.2, 9.66 Hz, H-3'), 4.19 (t, 1H, *J* = 3.2 Hz, H-4'), 3.85 (d, 1H, *J* = 11.88 Hz, H-6a), 3.74 (d, 1H, *J* = 11.88 Hz, H-6b), 3.66 (s, 2H, H-6'ab), 3.63 (m, 1H, H-5'), 3.61 (d, 1H, *J* = 7.83 Hz, H-2'), 3.57-3.54 (m, 2H, H-3,4), 3.47 (s, 1H, H-5), 3.35 (m, 1H, H-2). <sup>13</sup>C NMR (75 MHz, D<sub>2</sub>O): δ 133.2, 132.1, 130.2, 129.5, 128.7, 127.6, 127.4, 126.9, 126.7, 102.46 (C-1'), 87.0 (C-1), 80.0 (C-3'), 78.6 (C-5), 77.9 (C-3), 75.7 (C-4), 74.8 (C-5'), 71.5 (C-2), 69.0 (C-2'), 66.8 (C-4'), 60.8 (C-6'), 60.0 (C-6). ESI-HRMS: *m/z* calcd for C<sub>22</sub>H<sub>28</sub>O<sub>13</sub>S<sub>2</sub>, 564.0982; found 563.0909 [M-H].

**Table S1. Quantitation of ApoB100 N-glycan profiles after NEU2, NEU3, and NEU4 treatment ‡**

peak	RT	LDL	NEU2	Sia	NEU3	Sia	NEU4	Sia	LDL	NEU2	NEU3	NEU4
1	9.01	1.3%	0.0%	0.00	0.0%	0.00	0.0%	0.00	18.0%	24.4%	26.3%	8.0%
2	10.28	7.2%	8.2%	0.00	5.4%	0.00	2.6%	0.00				
3	11.47	4.7%	5.7%	0.00	5.0%	0.00	1.9%	0.00				
4	12.79	4.8%	10.5%	0.13	15.9%	0.22	3.4%	0.29				
5	14.20	4.8%	3.3%	0.50	2.2%	0.44	0.0%	0.00	48.6%	57.8%	62.8%	84.1%
6	15.49	15.4%	17.2%	0.55	24.5%	0.56	60.9%	0.50				
7	16.90	26.1%	34.4%	0.90	32.6%	0.88	23.2%	0.90				
8	18.23	1.5%	2.9%	1.00	3.5%	1.00	0.0%	1.00				
9	19.75	0.8%	0.0%	1.50	0.0%	1.50	0.0%	1.50				
10	20.91	4.0%	2.0%	1.40	2.1%	1.60	2.0%	1.67	30.5%	17.8%	10.9%	7.9%
11	22.18	23.5%	14.3%	2.14	7.8%	2.17	5.9%	2.17				
12	23.74	1.9%	0.0%	1.00	0.0%	1.00	0.0%	1.00				
13	24.94	1.2%	1.5%	2.00	1.0%	2.00	0.0%	2.00				
14	28.82	0.6%	0.0%	3.00	0.0%	3.00	0.0%	3.00	2.9%	0.0%	0.0%	0.0%
15	29.79	1.2%	0.0%	2.33	0.0%	2.33	0.0%	2.33				
16	31.03	1.0%	0.0%	3.00	0.0%	3.00	0.0%	3.00				

%change:           **0.0%**    **23.3%**    **33.6%**    **38.2%**

‡Percentages shown are normalized within each run. The average sialic acid content (Sia) was assigned using MS/MS fragmentation analysis to determine glycan structures found within each peak. The average number of Neu5Ac residues per peak was then used to sort into asialo-, monosialo-, disialo-, and trisialo-side groups. The total area of each group is totaled in the far-right columns for each sample. The % change in asialo+monosialo peaks is calculated in the bottom row. Abbreviations used: RT, retention time; Sia, sialic acid content.

**Table S2. Quantitation of ApoB100 N-glycan profiles after NEU1 treatment‡**

peak	RT	LDL	NEU1	Sia	LDL	NEU1
1	10.53	25.6%	36.0%	0.00	46.8%	62.8%
2	11.74	11.5%	15.5%	0.00		
3	13.17	9.8%	11.4%	0.00		
4	14.13	3.4%	3.7%	1.00	20.2%	18.4%
5	15.26	6.3%	6.1%	0.60		
6	16.71	10.5%	8.6%	0.67		
7	18.05	25.4%	17.5%	1.00	33.0%	18.8%
8	23.62	2.1%	0.0%	2.00		
9	25.34	5.5%	1.3%	2.00		

%change:                    **0.0%**                    **14.2%**

‡Percentages shown are normalized within each run. The average sialic acid content (Sia) was assigned using MS/MS fragmentation analysis to determine glycan structures found within each peak. The average number of Neu5Ac residues per peak was then used to sort into asialo-, monosialo-, disialo-, and trisialo-side groups. The total area of each group is totaled in the far-right columns for each sample. The % change in asialo+monosialo peaks is calculated in the bottom row. Abbreviations used: RT, retention time; Sia, sialic acid content.

**Table S3. Glycopeptides identified for control ApoB100**

Peptide mass	Peptide sequence	Glycosylation sites	Glycan structures assigned
<b>481.171</b>	(Y) GNCST (H)	<b>N158</b>	Hex6HexNAc3NeuAc1 Hex5HexNAc4NeuAc1 Hex5HexNAc3NeuAc1 Hex4HexNAc3NeuAc1 Hex5HexNAc4 Hex5HexNAc3 Hex6HexNAc3 Hex4HexNAc2 Hex3HexNAc2
<b>519.241</b>	(H) NGSEI (L)	<b>N4210</b>	Hex5HexNAc5NeuAc2
<b>535.254</b>	(A) MGNIT (Y)	<b>N3309</b>	Hex5HexNAc3 NeuAc1
<b>566.242</b>	(Y) SNASST (D)	<b>N956</b>	Hex5HexNAc4 NeuAc2
<b>566.257</b>	(N) QNFSA (G)	<b>N3074</b>	Hex5HexNAc4 NeuAc1
<b>594.237</b>	(S) NASSTD (S)	<b>N956</b>	Hex5HexNAc2
<b>594.237</b>	(G) GNTSTD (H)	<b>N1350</b>	
<b>607.268</b>	(I) GNGT TSA (N)	<b>N2752</b>	Hex9HexNAc2
<b>610.247</b>	(L) FNQSD (I)	<b>N3331</b>	Hex5HexNAc3NeuAc1
<b>610.283</b>	(I) DFNKS (G)	<b>N2212</b>	Hex5HexNAc4NeuAc1 Hex5HexNAc4NeuAc2
<b>610.294</b>	(L) RFNSS (Y)	<b>N1496</b>	
<b>612.262</b>	(G) AYSNAS (S)	<b>N956</b>	
<b>612.299</b>	(V) TKSYN (E)	<b>N3197</b>	Hex5HexNAc3NeuAc1
<b>670.286</b>	(E) NLSFSC (P)	<b>N7</b>	
<b>731.295</b>	(G) GNTSTDH (F)	<b>N1350</b>	Hex4HexNAc3NeuAc1 Hex4HexNAc4NeuAc1 Hex5HexNAc4NeuAc1 Hex5HexNAc4
<b>731.295</b>	(V) EGSHNST (V)	<b>N3384</b>	
<b>731.332</b>	(D) ANADIGNG (T)	<b>N2752</b>	
<b>731.332</b>	(G) SHNSTVS (L)	<b>N3384</b>	
<b>731.332</b>	(E) NVSLVCP (K)	<b>N7</b>	
<b>731.376</b>	(Y) NQNFSA (N)	<b>N3074</b>	
<b>750.378</b>	(E) NIDFNK (S)	<b>N2212</b>	
<b>750.389</b>	(S) NLRFNS (S)	<b>N1496</b>	Hex5HexNAc4NeuAc2 Hex5HexNAc4NeuAc1
<b>750.389</b>	(E) SNLRFN (S)	<b>N1496</b>	
<b>771.298</b>	(L) DTVYGNC (S)	<b>N158</b>	Hex5HexNAc3NeuAc1
<b>836.415</b>	(E) LFNQSDI (V)	<b>N3331</b>	Hex5HexNAc4NeuAc1 Hex5HexNAc4NeuAc2
<b>849.41</b>	(Y) NATWSASL (K)	<b>N3868</b>	Hex5HexNAc3NeuAc2

**Table S4. Glycopeptides identified for NEU3-treated ApoB100**

Peptide mass	Peptide sequence	Glycosylation sites	Glycan structures assigned
<b>363.151</b>	(Y) NET (K)	<b>N3197</b>	Hex5HexNAc5NeuAc1 Hex5HexNAc5
<b>594.237</b>	(S) NASSTD (S)	<b>N956</b>	Hex5HexNAc4
<b>594.237</b>	(G) GNTSTD (H)	<b>N1350</b>	Hex6HexNAc3 Hex5HexNAc2
<b>610.247</b>	(L) FNQSD (I)	<b>N3331</b>	Hex5HexNAc3NeuAc1
<b>610.283</b>	(I) DFNKS (G)	<b>N2212</b>	
<b>610.294</b>	(L) RFNSS (Y)	<b>N1496</b>	
<b>612.262</b>	(G) AYSNAS (S)	<b>N956</b>	Hex5HexNAc4
<b>612.299</b>	(V) TKSYN (E)	<b>N3197</b>	
<b>664.29</b>	(G) NGTTSAN (E)	<b>N2752</b>	Hex5HexNAc5
<b>656.271</b>	(D) TVYGNC (S)	<b>N158</b>	Hex5HexNAc5
<b>656.300</b>	(V) HNGSEI (L)	<b>N4210</b>	
<b>668.289</b>	(L) DTVYGN (C)	<b>N158</b>	Hex5HexNAc4NeuAc1
<b>674.274</b>	(G) NTSTDH (F)	<b>N1350</b>	Hex9HexNAc2
<b>674.310</b>	(D) ANADIGN (G)	<b>N2752</b>	
<b>674.372</b>	(M) LENVSL (V)	<b>N7</b>	
<b>681.269</b>	(Y) SNASSTD (S)	<b>N956</b>	Hex5HexNAc2 Hex5HexNAc4 Hex6HexNAc3
<b>731.295</b>	(G) GNTSTDH (F)	<b>N1350</b>	Hex4HexNAc4 Hex4HexNAc3 Hex5HexNAc4
<b>731.295</b>	(V) EGSNST (V)	<b>N3384</b>	
<b>731.332</b>	(D) ANADIGNG (T)	<b>N2752</b>	
<b>731.332</b>	(G) SHNSTVS (L)	<b>N3384</b>	
<b>731.332</b>	(E) NVSLVCP (K)	<b>N7</b>	
<b>731.376</b>	(Y) NQNFSAG (N)	<b>N3074</b>	
<b>750.378</b>	(E) NIDFNK (S)	<b>N2212</b>	Hex5HexNAc4 Hex5HexNAc4NeuAc1
<b>750.389</b>	(S) NLRFNS (S)	<b>N1496</b>	
<b>750.389</b>	(E) SNLRFN (S)	<b>N1496</b>	
<b>761.342</b>	(A) NADIGNGT (T)	<b>N2752</b>	Hex5HexNAc5
<b>836.415</b>	(E) LFNQSDI (V)	<b>N3331</b>	Hex5HexNAc4 Hex4HexNAc3

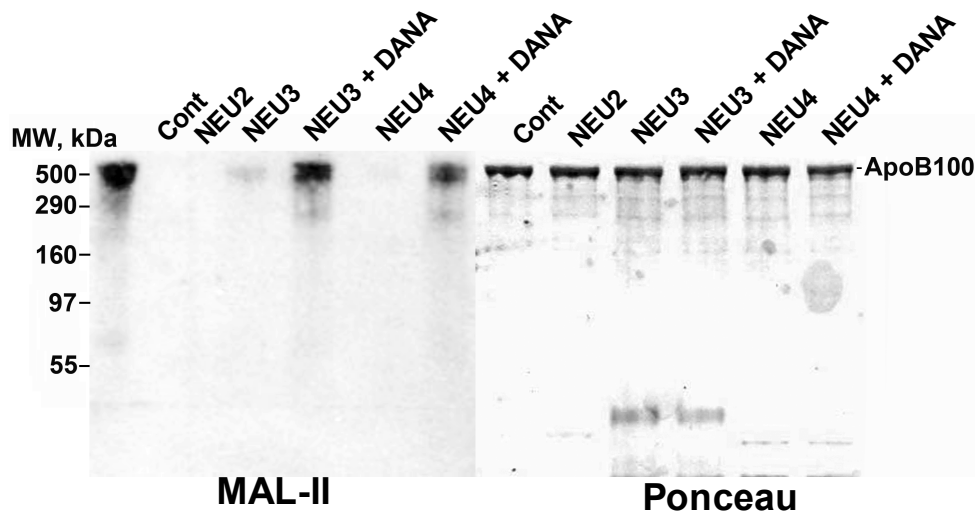


**Figure S1. Pan-neuraminidase inhibitor DANA prevents desialylation of ApoB100 in LDL by neuraminidases.**

Purified human LDL were incubated with human recombinant NEU2,3 or 4 either with or without pan-neuraminidase inhibitor DANA (1 mM final concentration) and glycosylation of ApoB100 was analyzed by blotting with MAL-II lectin. Ponceau S-stained membrane was used as a control for protein loading. Abbreviations used: ApoB, Apolipoprotein B 100; DANA, 2,3-didehydro-2-deoxy-N-acetyl-neuraminic acid; LDL, low-density lipoprotein; MAL, *Maackia amurensis* lectin.



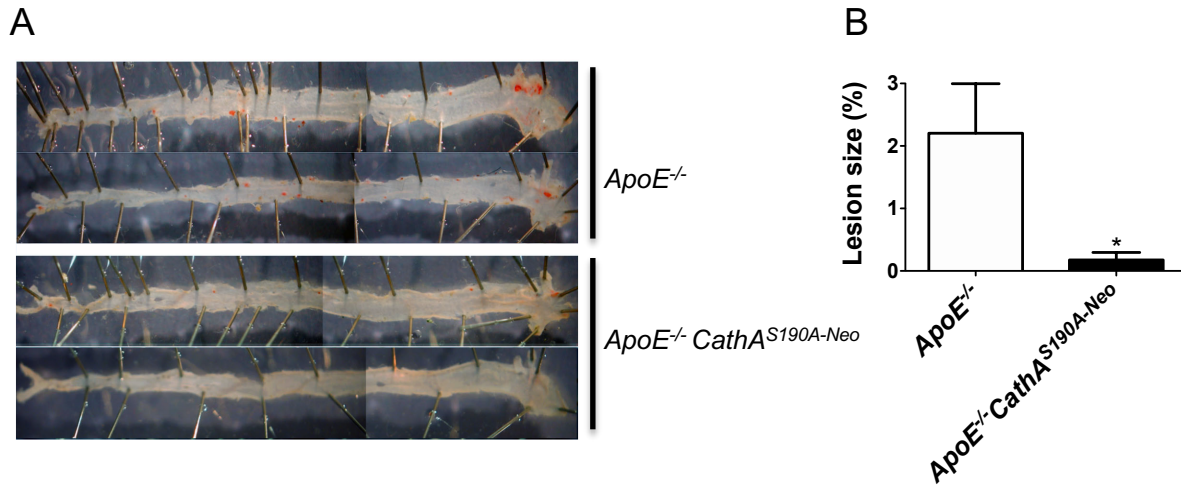


**Figure S2. NEU1 deficiency reduces atherosclerotic lesions in the thoracic aorta of *ApoE*<sup>-/-</sup> mice**

(A) Representative photomicrographs of Red Oil O-stained fatty streaks in the intima of the thoracic aorta and (B) quantitative analysis of atherosclerotic lesion sizes.

For the *en face* analysis of the whole aorta *ApoE*<sup>-/-</sup> and *ApoE*<sup>-/-</sup>*CathA*<sup>S190A-Neo</sup> female mice fed with a normal diet were euthanized at 20 weeks and their aorta dissected out from the heart until 3-5 mm after the iliac bifurcation. Fat and connective tissue were removed, and the heart and aortic arch separated from the aorta. The remaining aorta was opened longitudinally and pinned on silica Petri dish using 0.2-mm-diameter stainless steel pins (Fine Science Tools). The pinned vessels were stained the Sudan IV (Sigma-Aldrich, St. Louis, MO, USA). The images were captured with a PixeLINK PL-A686C camera attached to a Leica MZ6 dissecting microscope. The area of stained lesion size was determined using ImageJ analysis software. Bar graph shows mean values and SEM of data from 6 mice for each genotype; \* statistically different from *ApoE*<sup>-/-</sup> mice ( $p < 0.05$ ) according to t-test.

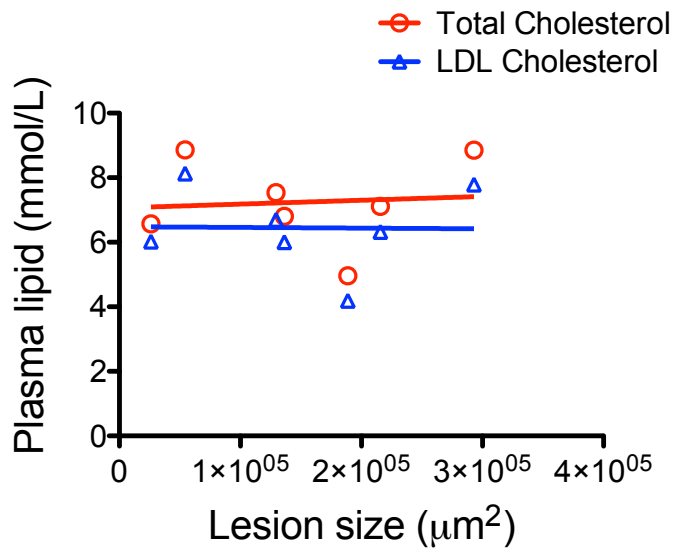


**Figure S3. Plasma levels of total and LDL cholesterol and atherosclerotic lesion size in the heart sinus of individual *Apoe*<sup>-/-</sup>*Neu3*<sup>-/-</sup> mice**

No correlation was observed between the size of fatty streaks and LDL or total cholesterol plasma levels. For both values the slope of linear regressions is not significantly different from zero. Abbreviations used: LDL, low-density lipoprotein; Neu, neuraminidase

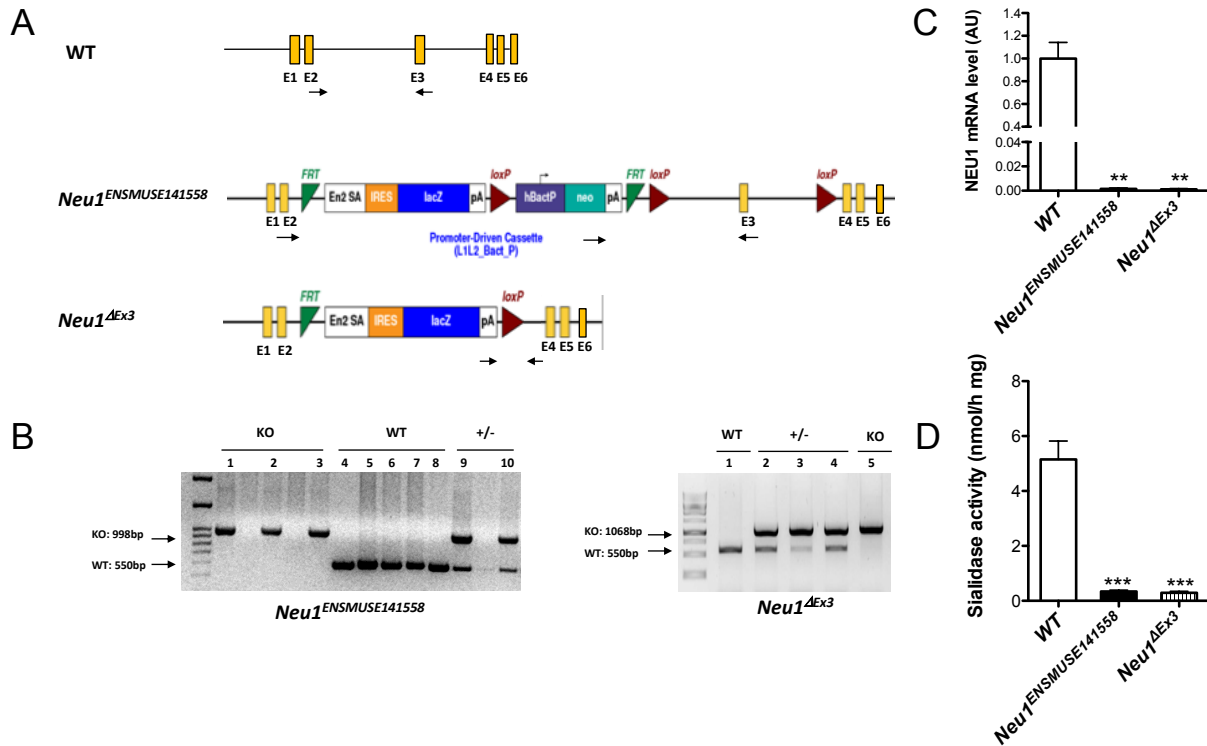


**Figure S4. Generation of *Neu1* KO mouse strains**

(A) The targeted *Neu1*<sup>ENSMUSE141558</sup> allele contains *LacZ/BactPNeo* cassette inserted into the intron 2 of the mouse *Neu1* gene, resulting in the expression of a fusion protein containing the mouse NEU1 amino acid sequence encoded by the exons 1-2 followed by the bacterial  $\beta$ -galactosidase encoded by the *LacZ* gene under the control of the endogenous *Neu1* promoter.<sup>24</sup> In addition the exon 3 of the gene is flanked with *LoxP* sites. The *Neu1*<sup>ΔEx3</sup> strand was obtained by crossing the *Neu1*<sup>ENSMUSE141558</sup> mouse with C57Bl6J mice with global constitutive expression of Cre recombinase resulting in removal of the entire exon 3 from the *Neu1* gene.

(B) The *Neu1*<sup>ENSMUSE141558</sup> and *Neu1*<sup>ΔEx3</sup> mice from F2 generation were genotyped by PCR with primers shown in (A) that amplify 998 and 1068 bp fragments from the targeted alleles and 550 bp fragment from the WT allele.

(C) Neu1 mRNA level was measured by RT-QPCR in kidney tissue of mice homozygous for the targeted allele is reduced to less than 0.15% i.e. below the detection level. Three mice were studied for each genotype. \*\* - significantly different from WT mice ( $p < 0.01$ ) in Kruskal-Wallis followed by Dunn's multiple comparisons test.

(D) Residual neuraminidase activity in kidney tissue from mice homozygous for the targeted alleles is reduced to 3% of that in the WT similar to that in the previously reported *Neu1* KO mouse. Abbreviations used: Neu, neuraminidase.<sup>46</sup> Three mice were studied for each genotype. \*\*\* - significantly different from WT mice ( $p < 0.001$ ) in Kruskal-Wallis followed by Dunn's multiple comparisons test.

Name	Structure	Reference		Conc used [mg/kg BW]	Selectivity
DANA		78	DANA	30	NEU3/4; 4X
CG17701		12	7i	1	NEU3/4; 45X
CG22601		12	8b	10	NEU3; 10X
CG14601		79	11c	10	NEU1; 33X
C9-BA-DANA		79, 53	8, 10h	30	NEU1; 32X

**Figure S5. Pharmacological inhibitors of human NEU used in this study.**

Compounds used in this study are summarized with literature references and reported selectivity for NEU enzymes. Compound C9-BA-DANA was originally named as a C9-butylamido compound, although it should be referred to as a pentyl amide derivative. We have kept this abbreviation for consistency with the literature. Structures are shown in the C1 methyl ester forms used for this study. Carbon atom numbering used for abbreviations is shown on the structure for DANA. The designations for compounds are shown from original references.

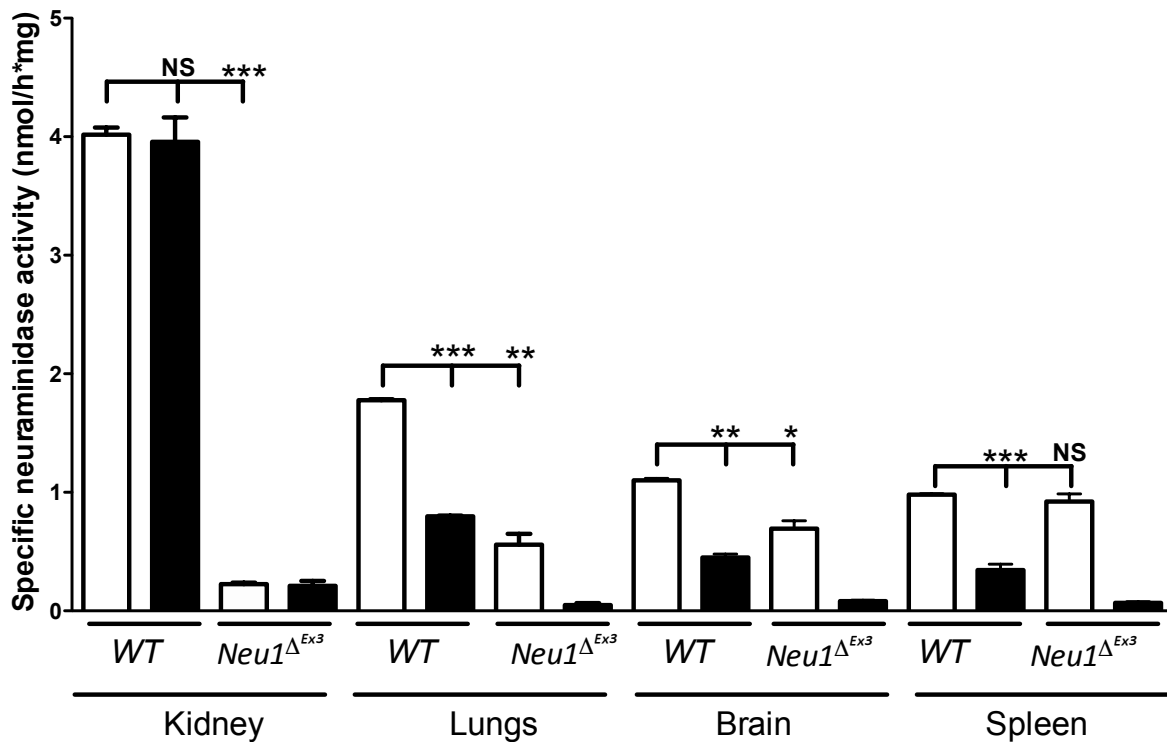


**Figure S6. NEU1 isoform is responsible for the majority of acidic neuraminidase activity in the mouse kidney**

Acidic neuraminidase activity was measured in the homogenates of *Neu1*<sup>ΔEx3</sup> mice and their WT siblings using the fluorogenic substrate 4-methylumbelliferone-N-acetyl-neuraminic acid and in the absence (total neuraminidase activity) or the presence (NEU1 specific activity) of a specific neuraminidase 3 and 4 inhibitor, C9-4BPT-DANA (CG17701).<sup>12</sup> In contrast to that in lungs, brain and spleen, total neuraminidase activity in kidney tissues is not inhibited by C9-4BPT-DANA and is reduced almost to the background level in the kidney from *Neu1*<sup>ΔEx3</sup> mice. Data are shown as means of experiments ( $\pm$ SD) performed using 3 mice per genotype. Significant (\* $P < 0.05$ , \*\* $P < 0.01$ , \*\*\* $P < 0.001$ ) determined by ANOVA with a Tukey's post-test. Abbreviations used: Neu, neuraminidase

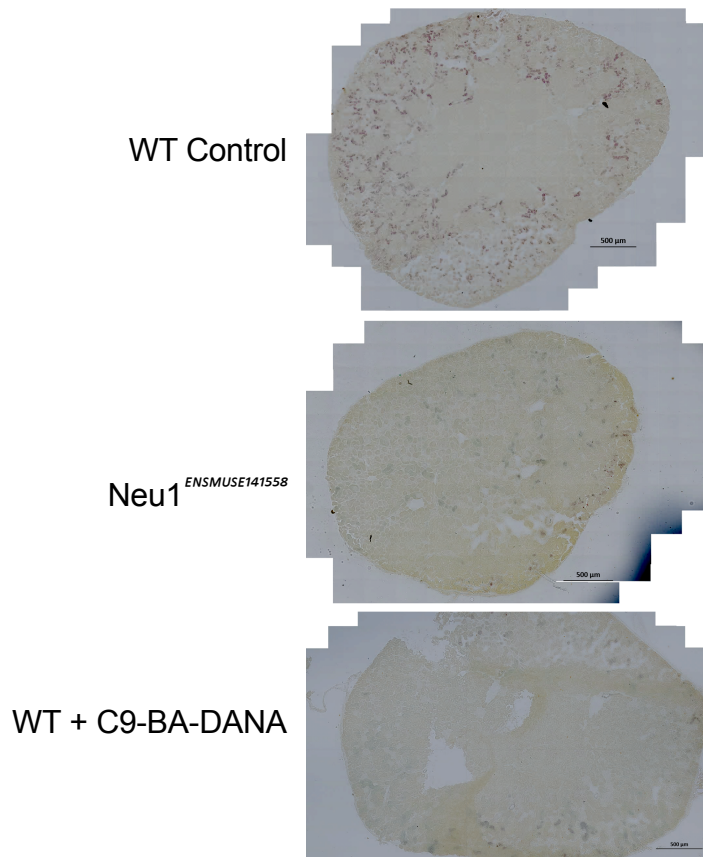


**Figure S7. In vivo treatment of mice with a specific NEU1 inhibitor C9-BA-DANA blocks neuraminidase activity in kidney tissues**

Four week-old WT mice were injected intraperitoneally with C9-BA-DANA (30 mg/kg) or saline for 2 consecutive days. NEU1 KO *Neu1*<sup>ENSMUSE141558</sup> mice were receiving saline injections only. Twenty hours after the last injection mice were sacrificed and their kidney removed and frozen in OCT. Five μm thick sections were stained with histochemical neuraminidase substrate, X-Neu5Ac. Tissue of saline-treated WT mouse but not of C9-BA-DANA-treated WT or NEU1 KO mouse shows staining the neuraminidase substrate. Panels show representative images of triplicate experiments. Abbreviations used: Neu, neuraminidase